December 2012

Structure and Chemistry of Model Catalysts in Ultrahigh Vacuum

Joshua D. Walker
University of Wisconsin-Milwaukee

STRUCTURE AND CHEMISTRY OF MODEL CATALYSTS IN ULTRAHIGH VACUUM

by

Joshua D. Walker

A Thesis Submitted in

Partial Fulfillment of the

Requirements for the Degree of

Master of Science

in Chemistry

at

The University of Wisconsin-Milwaukee

December 2012

ABSTRACT

STRUCTURE AND CHEMISTRY OF MODEL CATALYSTS IN ULTRAHIGH VACUUM

by

Joshua D. Walker

The University of Wisconsin-Milwaukee, 2012
Under the Supervision of Professor W. T. Tysoe

The study of catalysis is a key area of focus not only in the industrial sector but also in the nature and biological systems. The market for catalysis is a multi-billion dollar industry. Many of the materials and products we use on a daily basis are formed through a catalytic process. The quest to understanding and improving catalytic mechanisms is ongoing. Many model catalysts use transition metals as a support for chemical reactions to take place due to their selectivity and activity. Palladium, gold, and copper metals are studied in this work and show the ability to be catalytically reactive. It is important to understand the characteristics and properties of these surfaces. A well-known example of catalysis is the conversion of carbon monoxide (CO), a very harmful gas to carbon dioxide (CO_2) which is less harmful. This reaction is mainly seen in the automotive industry. This reaction is investigated in this work on a Au(111) single crystal, which is normally inert but becomes reactivity with the adsorption of oxygen on the surface. Temperature Programmed Desorption (TPD) is used to understand some of the chemistry

and effects with and without the addition of H_2O. The oxidation of CO is shown to be enhanced by the addition of water, but warrants further analysis too fully understand the different mechanisms and reaction pathways existing.

The field of nano-electronics is rapidly growing as technology continues to challenge scientists to create innovative ideas. The trend to produce smaller electronic products is increasing as consumer demands persist. It has been shown previously that 1,4-phenlyene diisocyanobenzene (1,4-PDI) on Au(111) react to form one-dimensional oligomer chains comprising alternating gold and 1,4-PDI units on the Au(111) surface. A similar compound 1,3-phenlyene diisocyanobenzene (1,3-PDI) was studied in order to investigate whether the oligomerization found for 1,4-PDI is a general phenomenon and to ultimately explore the effect of molecular geometry on electron transport using a range of surface-sensitive techniques.

Sulfur-containing molecules, in particular those with sulfur-sulfur linkages, are used as lubricant additives for ferrous surfaces[1-14] so that dialkyl disulfides have been used as simple model compounds to explore the surface and tribological chemistry on iron [15,16] where they react at the high temperatures attained at the interface during rubbing to deposit a ferrous sulfide film. However, the tribological chemistry can depend critically on the nature of the substrate so that a good lubricant additive for one type of surface may not be applicable to another. In particular, the lubrication of sliding copper-copper interfaces in electrical motors [17-20] provides a particular challenge. To study this system surface sensitive techniques Low energy electron diffraction (LEED) and TPD surface analysis was employed. LEED experiments suggest that tribological

experiments can be conducted on copper foils rather than copper single crystals and produce comparable results.

The ability to produce ideal model catalysts is very important in the Surface science field. To enhance catalytic performance of these catalysts, various strategies can be used in the preparation process. One approach in this quest is to produce an alloy surface that increases the activity of the surface. The process of developing and understanding the chemistry of AuPd alloys was probed in detail using TPD, LEED and Density Functional Theory (DFT).

TABLE OF CONTENTS

LIST OF FIGURES

Figure 6.8 Plot of the yield of water against the yield of oxygen following exposure of carbon monoxide to Au(111) surface covered with 0.5 monolayers of atomic oxygen and then exposed to water to form surface hydroxyl groups.

Figure 6.9 TPD profiles collected at 44 amu following exposure of carbon monoxide to Au(111) surface covered with atomic oxygen and then exposed to water to form surface hydroxyl groups, collected using a heating rate of 3.4 K/s. A. 4L O_2, 0.05L H_2O, .25L CO (θ(OH)= 0.12 ML), B. 8L O_2, 0.1L H_2O, 0.5L CO (θ(OH)= 0.29 ML), C. 11L O_2, 0.2L H_2O, 0.6L CO (θ(OH)= 0.41 ML), D. 15L O_2, 0.25L H_2O, 0.75L CO (θ(OH)= 0.56 ML), E. 22L O_2, 0.35L H_2O, 0.85L CO (θ(OH)= 0.82 ML), F. 30L O_2, 0.5L H_2O, 1L CO (θ(OH)= 1.11 ML), G. 45L O_2, 0.65L H_2O, 1.25L CO (θ(OH)= 1.67 ML), H. 60L O_2, 0.75L H_2O, 1.5 L CO (θ(OH)= 1.8 ML), I. 100L O_2, 1L H_2O, 1.75L CO (θ(OH)= 2.0 ML).

ACKNOWLEDGEMENTS

I would like to thank my advisor, Professor Wilfred T. Tysoe, not only for his invaluable guidance and assistance, but also for his vision and dedication to enhancing my knowledge in the scientific area. I would also like to thank my committee members Professors Dennis W. Bennett and Carolyn R. Aita for their advice and insight.

To the many members of Professor Tysoe's group whom I have worked with during my time at UWM, your assistance has been priceless. I have made lifelong friends throughout this entire process. I have really enjoyed teaching and learning from you. I would also like to thank the UWM Chemistry and Biochemistry department, faculty, staff and all other fellow graduate students for your support; you were really there when I needed you the most and ensured that my academic experience here was a success.

Finally I would like to dedicate this work to my late father Jimmy D. Walker and my mother Betty S. Walker; you have helped me throughout my life and made countless sacrifices to ensure that I became a successful person. I am very grateful to have you as parents and your love, patience and guidance is deeply appreciated. To a host of family and friends I would like to thank you for your support and encouragement. Last but not least I would like to thank my Lord and Savior Jesus Christ.

Chapter 1: Introduction

1.1 Surface Science and Catalysis

Surface science is the study of physical and chemical phenomena that occur at the boundary of two phases, including solid–liquid, solid–gas, solid–vacuum, liquid-gas and solid-solid interfaces. Surface science studies cover a wide range of shapes, sizes and textures of surfaces. Surfaces have multiple layers and sites which can display variable environments that may produce different reactivity and behavior. The development of surface techniques to study gas-phase molecular processes in the early 1950s sparked an interest in the studies of surfaces on a molecular level. The availability of economical ultrahigh vacuum systems (UHV) which was initially developed for space research provided new opportunities for a diverse range of research areas. With the development of UHV systems clean surfaces could be studied for the first time, as a result a wide-range of surface characterization techniques were soon to follow. Surface phenomena such as adsorption, bonding, catalysis, diffusion, friction, lubrication, oxidation, and thin-film growth to name a few are being studied on a molecular scale [1]. Surface science is increasingly being bridged and connected to other science disciplines. Research in surface science has contributed to high-technology areas of semiconductors, chemical sensors, polymer surfaces, metal composites, and new areas of electrical, magnetic and optical devices. Surface science has become one of the main disciplines of chemistry.

Catalysis is a process in which the chemical reaction rate is accelerated by a small amount of chemical substance known as a catalyst. The catalyst may contribute to the

reaction, but is not consumed by the reaction itself. Catalysts which speed up a reaction are called positive catalyst and one which in turn slows down reactions are inhibitors or negative catalysts. Catalysts are not only found in industrial applications but also in nature as well. Enzymes are found in the human body and act as catalysts for essential processes such as metabolism and catabolism. Catalysis on the industrial level is very important in the manufacture of many products that are used on a daily basis. It has been estimated that 90% of all commercially produced chemical products involve catalysts at some stage in the process of their manufacture. [2] In 2005, catalytic processes generated about $900 billion in products worldwide [3]. Catalysts are found in the process of producing bulk and fine chemicals, energy, food, and pesticides just to name a few. Catalysts are usually defined as either homogeneous or heterogeneous, depending on whether a catalyst exists in the same phase as the substrate. Homogeneous catalysts function in the same phase as the reactants. Typically homogeneous catalysts are dissolved in a solvent with the substrates. Heterogeneous catalysts act in a different phase than the reactants. Most heterogeneous catalysts are solids that act on substrates in a liquid or gaseous reaction mixture [4]. There are three vital steps in the heterogeneous catalysis process which include the adsorption of reactants on a surface, reaction, and desorption of the products. These steps are the main focus of the work presented in this thesis.

Overview of Thesis

Chapter 1: Discusses some background information on Surface Science and Catalysis, and a brief summary of the thesis work presented.

Chapter 2: Describes the experimental methods and techniques used in this work. Specific equipment and processes were reviewed and discussed.

Chapter 3: Focuses on understanding structural changes and order of Au/Pd(100) alloys using LEED.

Chapter 4: Adsorption of 1,3-Phenylene Diisocyanide on Au(111).

Chapter 5: Describes the LEED Characterization of Cu Foils.

Chapter 6: Concentrates on the Adsorption of Oxygen and Water and CO Oxidation on Au(111)

References

[1] Recognizing the in Best Innovation: Breakthrough Catalyst. *R&D Magazine,* (2005) 20

[2] Chevronwithtechron.com/products/documents/Diesel_Fuel_Tech_Review

[3] Modern Techniques of Surface Science: D. P. Woodruff, T. A. Delchar

[4] O. Furlong, Ph.D thesis, University of Wisconsin-Milwaukee, **2010**

Chapter 2: Experimental Methods and Techniques

2.1 Introduction

To perform surface science experiments, it is very important to start with a clean surface. The quest to maintain a clean surface for extended time periods is possible with ultra-high vacuum (UHV) conditions. UHV conditions are required since molecules in the air rapidly adsorb onto the surface at atmospheric pressures. While doing experiments ideally a background pressure of at least 5×10^{-10} Torr is desirable to minimize contamination. Working under UHV conditions allow for various surface sensitive and characterization techniques to be used. Techniques such as Low Energy Electron Diffraction (LEED), Auger Electron Spectroscopy (AES), Temperature Programmed Desorption (TPD), and Mass Spectroscopy (MS) were used in the work presented. Also other instrumentation and methods used during experiments will be discussed in more detail.

2.2 Experimental Methods

2.2.1 UHV Systems and Equipment

A common UHV system is comprised of a stainless-steel chamber with several flanged ports of different sizes, to which the required equipment can be connected. Leak valves, manipulators, viewports, evaporation sources, surface cleaning equipment, etc can

be attached to a chamber via the ports. An example of a typical UHV chamber is shown in Figure 2.1.

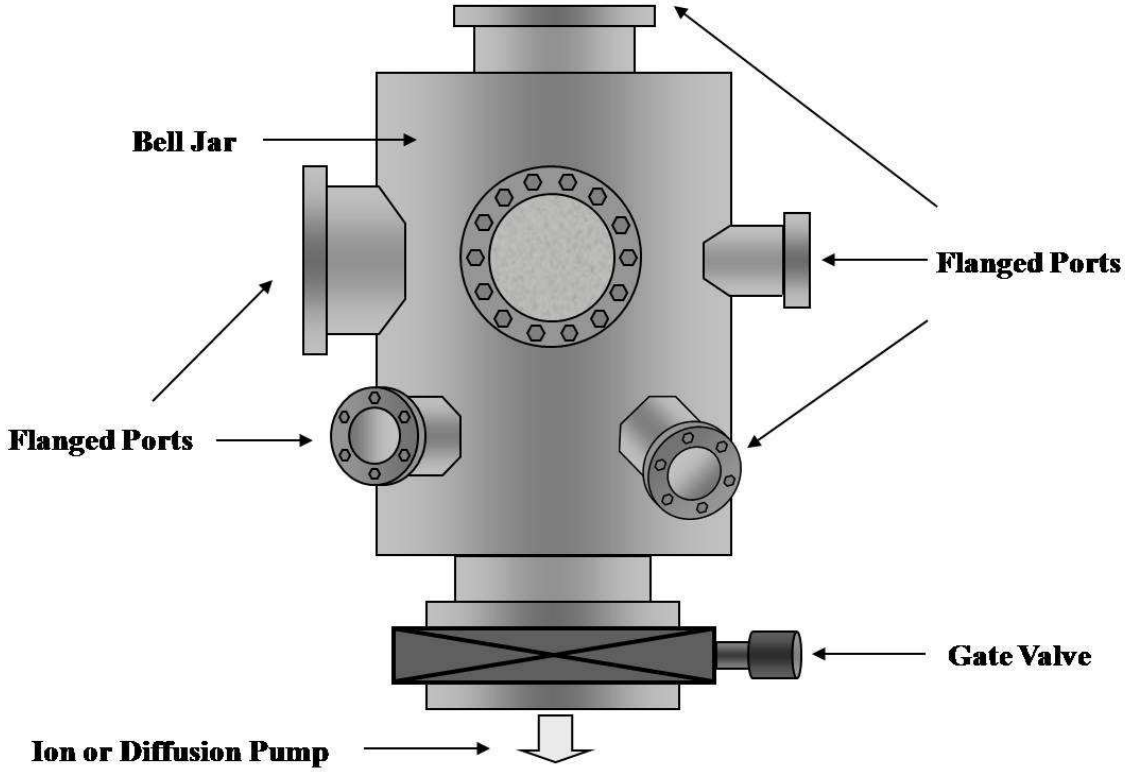

Figure 2.1. UHV Chamber

2.2.1 Vacuum Pumps

Various pumps are used to obtain UHV conditions, and usually a combination of pumps is used simultaneously. Usually a mechanical pump and either a diffusion, ion or turbomolecular pump are used in unison depending on the experimental application. The following vacuum pumps discussed were used in this work.

2.2.1.2 Mechanical (Rotary) Pumps

Mechanical pumps or rotary pumps operate by cycling fluid using the principles of rotation. As this rotation proceeds, a vacuum is created which traps gas and forces it from the inlet to an outlet of the pump. Oil is the common fluid in a mechanical pump, which also helps to lubricate the moving parts. In (Figure 2.2), the operation of common rotary pumps is illustrated. Mechanical pumps are frequently used on gas lines to remove any air; it is also used commonly as a backing pump for diffusion or turbomolecular pumps. Mechanical pumps can normally only reach a vacuum pressure of about 1×10^{-3} Torr when operated at ideal speeds to minimize wear [1]. Mechanical pumps are essential to operating a common UHV system.

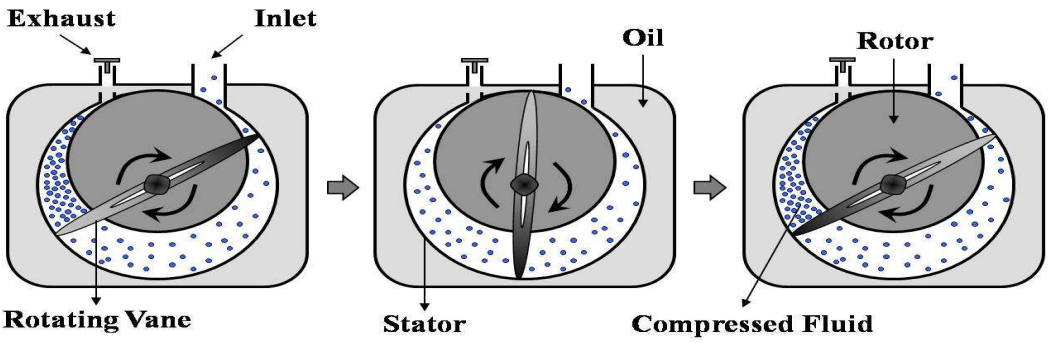

Figure 2.2. Diagram of the mechanical pumping process.

2.2.1.3 Diffusion Pumps

Diffusion pumps where first presented in 1915 by Wolfgang Gaede using mercury vapor [2] and they were the first type of high vacuum pumps operating in the regime of free molecular flow, where the movement of the gas molecules can be better understood as diffusion than by conventional fluid dynamics. Diffusion pumps are widely used for

the operation of UHV chambers. A diffusion pump can reach a magnitude of pressure 1×10^{-10} Torr or lower when using a liquid nitrogen (LN_2) cold trap. A diffusion pump is very durable and efficient mainly due to the lack of moving parts. The operation of a diffusion pump is very simple. The pump is a circular stainless steel apparatus containing oil, jet assemblies, and water cooling coils, electric heater, gate valve and cryotrap. As the oil is heated, it begins to vaporize, and then moves upward and then is forced downward through the jet assemblies capturing molecules in the background and driving them away from the chamber. Cryotraps are essential to store LN_2 and to help prevent back streaming of oil into the chamber from the diffusion pump, which can cause severe problems. The advantages of diffusion pumps easily outweigh the disadvantages. A detailed schematic of a diffusion pump is shown in (Figure 2.3-a)

2.2.1.4 Turbomolecular Pumps

The turbomolecular pump was invented in 1958 by Becker, based on the older molecular drag pumps developed by Gaede in 1913, Holweck in 1923 and Siegbahn in 1944, [3]. A turbomolecular or turbo pump is used to obtain and maintain high vacuum. Turbo pumps work on the principle that gas molecules can be given energy in a preferred direction by repeated collision with a moving solid surface (rotary blades). In a turbomolecular pump, a rapidly spinning turbine rotor collides with gas molecules from the inlet of the pump towards the exhaust in order to create or sustain a vacuum shown below in (Figure 2.3-b). Turbo pumps do not require the use of oil which means it remains relatively clean and can operate over vacuum pressure ranges from 1×10^{-3} to 2×10^{-11} Torr. Some of the drawbacks of turbomolecular pumps are the requirement of

very high grade bearings which can become expensive, they are not efficient at pumping small molecules, and a larger backing pump is needed to work efficiently.

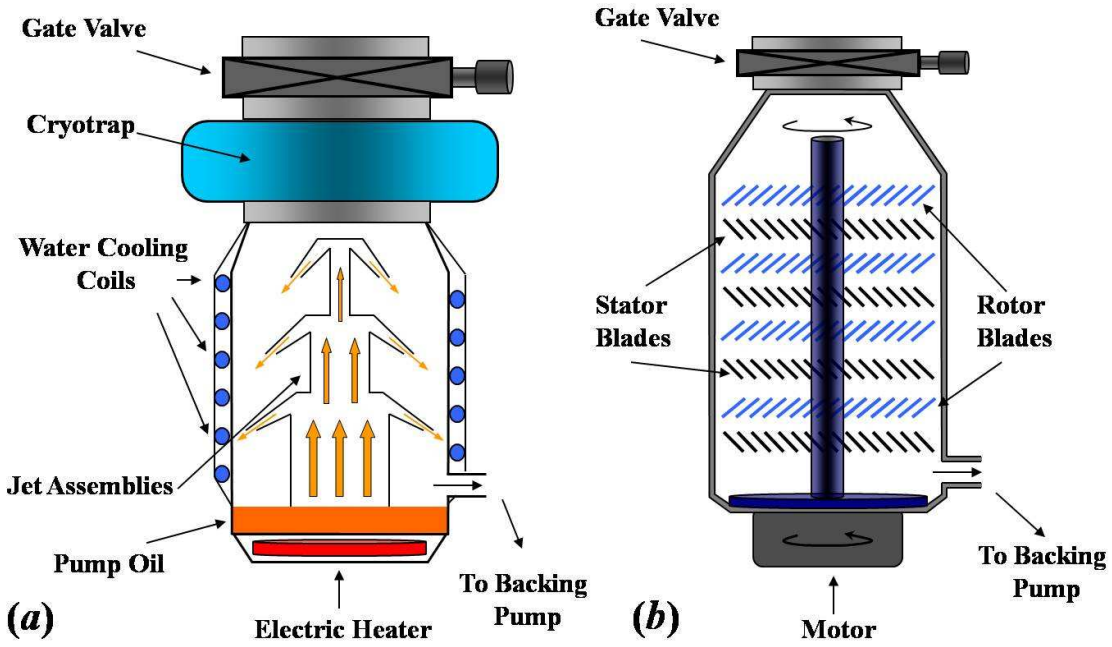

Figure 2.3. Illustrations of Diffusion and Turbo pumps

2.3 Sample Manipulators and Mounting

There are a wide range of sample manipulators that can be used on UHV systems depending on the experimental setup. There were two types of manipulators used in this thesis. The first manipulator is a Huntington Model PM-600-XYZR which is shown in (Figure 2.4). The manipulator allows for the sample to be moved in either the x,y and z directions. The sample can be rotated through 360˚ to access the various experimental instruments. This manipulator was primarily used on a TPD UHV chamber; it was also

equipped with a LN_2 cooling system. The LN_2 system allows the sample to be cooled to ~80 K which gives the ability to do surface analysis over a wide range of temperatures.

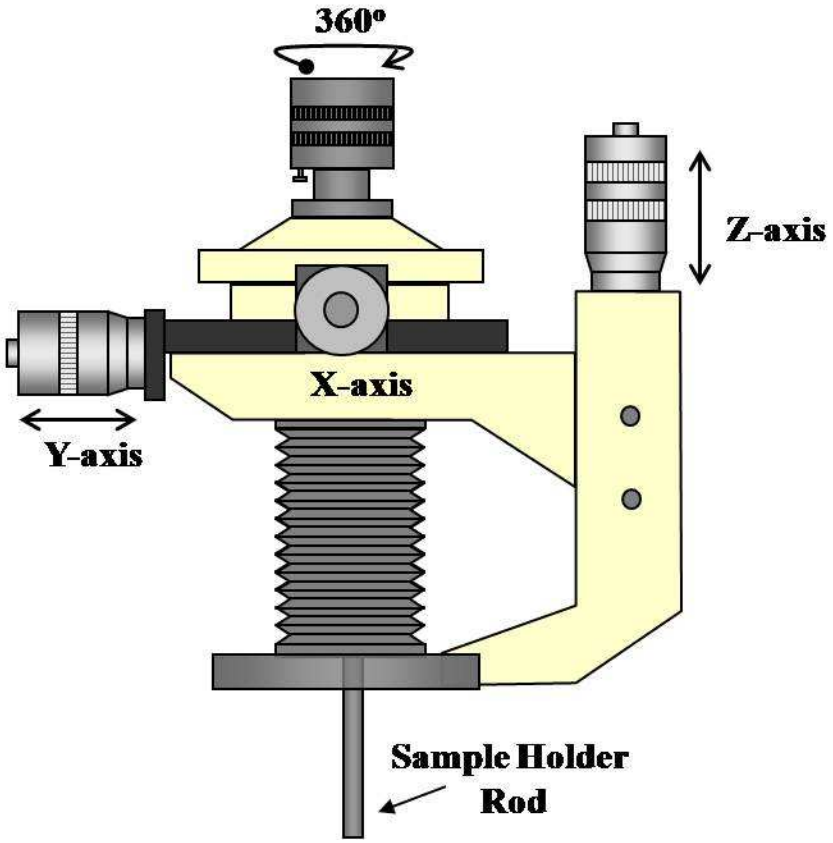

Figure 2.4. Sample Manipulator

The second type of manipulator used in this thesis was a Vacuum Generators type – DPRF which was in a Low-energy electron diffraction (LEED) chamber. This manipulator was differentially pumped and was equipped to be lowered into a special cell for high-pressure experiments. The research conducted in this thesis was on pure

palladium (100), palladium (111) single crystals, a Au(111) single and Cu foils. The samples were mounted using 0.5mm diameter Ta heating wires wrapped around the crystals, which was then spot-welded to 2 mm Ta heating posts. To properly measure sample temperatures, K-type thermocouple wires (Chromel+, Alumel-) were spot- welded to the back of the sample. Once the sample is secure it is then attached to the manipulator rod which is connected to the controls were the sample position can be adjusted. (Figure 2.5) shows diagram of a sample mounted for experiments. There are various sample mounting orientations possible depending on the nature of the experiment. When using the liquid nitrogen cooling system, the liquid is pumped through a ceramic insulated feedthrough by a small mechanical pump. The excess nitrogen gas is pumped from the cooling system throughout the exhaust. Sample mounting a single crystal is a delicate process which requires the sample to be free to move inside the chamber without any restrictions.

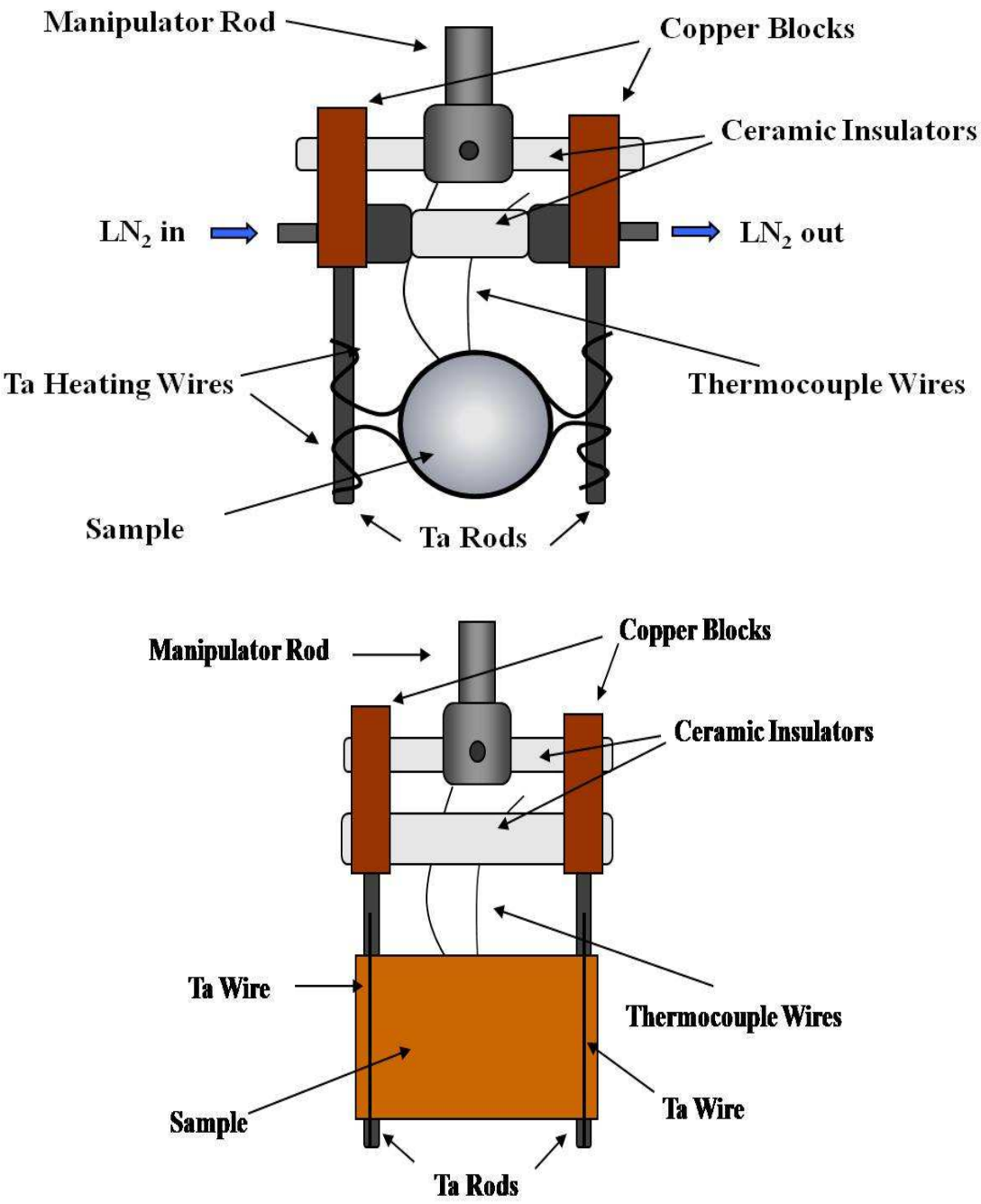

Figure 2.5. Diagram of Sample Holders

2.3.1 Sample Cleaning and Preparation

There are several steps involved in the cleaning and preparation of the Pd(100), Pd(111), Au(111) and Cu foil samples. With a new Pd single crystal sample it takes numerous cleaning cycles and heating procedures to remove carbon from the bulk. The standard cleaning methods included several cycles of Argon ion bombardment, and annealing the sample to ~1100 K. Also heating in oxygen is used to remove carbon, this consists of dosing oxygen at a background pressure of ~ 3×10^{-8} Torr while heating the sample to ~800-950 K for various time periods. To check the cleanliness of the sample Auger Electron Spectroscopy (AES) and Temperature-programmed desorption (TPD) techniques were used. The Au(111) single crystal was cleaned by several Argon bombardment cycles, also absorbing ozone onto the surface at a background pressure of ~3×10^{-8} Torr, then checking the cleanliness of the sample by AES and TPD. The Cu foils were cleaned in a similar manner with several Argon ion bombardment and heating cycles. The cleanliness of the samples was monitored using Auger electron spectroscopy. All samples were cleaned in a UHV environment.

2.3.2 Au Evaporation Source

For some experiments a gold evaporation source was used to grow a thin film of gold on the Pd(100) or Pd(111) crystals. The gold source must first be outgassed for several hours before a clean film can be deposited onto the sample. After the degassing has taken place and the sample is thoroughly cleaned, a thin film of gold several monolayers thick is evaporated onto the sample. The design of the evaporation source originally created by Lambert et al. [4] is shown in (Figure 2.6)

below. To produce certain AuPd alloys, a Palladium sample containing ~5 monolayers (ML) of gold is annealed to various temperatures, which allows the gold to diffuse into the bulk of the palladium sample in a controlled way to create various alloys. The gold evaporation source was a key tool in several experimental processes.

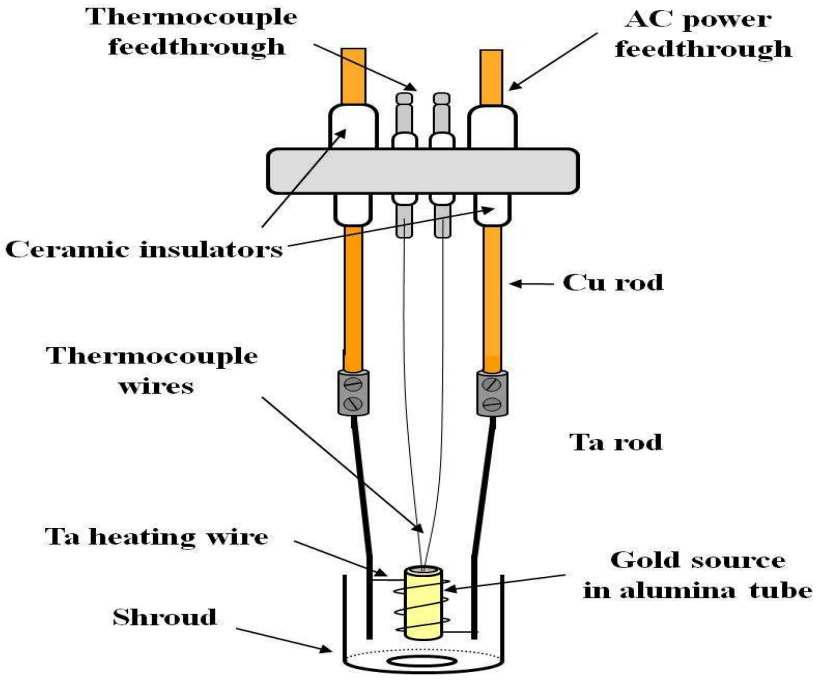

Figure 2.6. Thin film evaporation source

2.3.3 Gas Handling Line and Chemical Purification

In order to purify, store and prepare gases introduced into the UHV system for experiments, a glass gas handling line was used. A schematic of the gas handling line is shown in (Figure 2.7). The glass line consisted of a cold cathode gauge for measuring pressure, a diffusion pump which is back-pumped by a mechanical rotary pump to keep contaminants out of the gas line. Two variable leak valves connect the gas line to the

UHV chamber. Leak valves were used to introduce various gases or vapors to the vacuum chamber depending on the experiment. A manometer was used to measure gas pressures between 1 mTorr and 1.5 atm. For the handling of the chemical compounds and gases most substances were transferred to glass vials or attached directly to the gas line via a gas cylinder. Liquids were purified more thoroughly by freeze-pump-thaw cycles. The purity of the reactants was monitored by mass spectrometry.

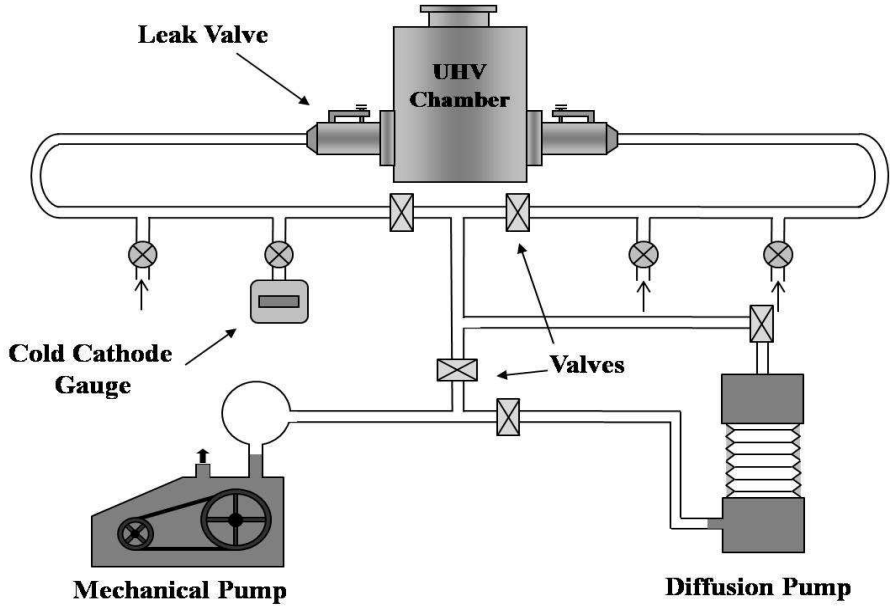

Figure 2.7. Representation of gas line handling system.

2.3.4 Cylindrical Mirror Analyzer (CMA)

A CMA is an electron analyzer that can be used to collect Auger spectra. A CMA consists of two concentric metal cylinders arranged such that their axes are coincident [5]. A simple illustration of a single pass CMA is shown in (Figure 2.8). A voltage difference is placed between the cylinders such that there is an electric field between

them. Electrons are injected from a point on the axis into the gap between the two cylinders between which a potential is applied with very high energy, they will impinge on the outer cylinder (which has negative voltage (-)). The electrons that have too low of an energy will be attracted to the inner cylinder which is at ground potential. Therefore only electrons within a narrow energy region (called the pass energy) can progress all the way along the cylinders to the detector.

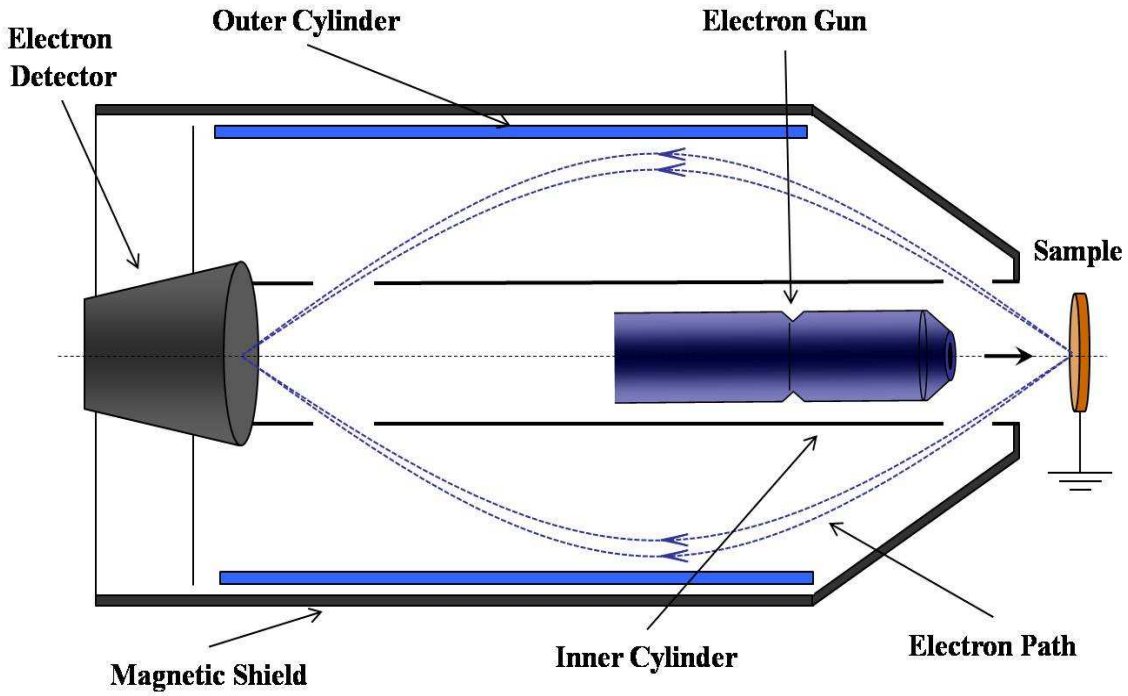

Figure 2.8. Diagram of single pass Cylindrical Mirror Analyzer

Most commercial CMA's are usually based on a "double pass" design where electrons travel through two analyzers placed in series. The path of travel for the electrons is then in the shape of a figure-of-eight. This additional stage of filtering is incorporated to diminish noisy background signals due to secondary electrons generated within the analyzer.

2.3.5 Knudsen Source

Most molecules in this work were introduced from standard gas handling line via a UHV variable leak valve. Certain molecules used in these experiments were either too reactive or did not have ample vapor pressure and for these molecules used a Knudsen source as designed (Figure 2.9), which was backed by a turbomolecular pump. The compounds could be submerged in ice, to lower their vapor pressure introduced to the chamber at room temperature, or heated to a specific temperature depending on the vapor pressure or coverage desired for the experiment.

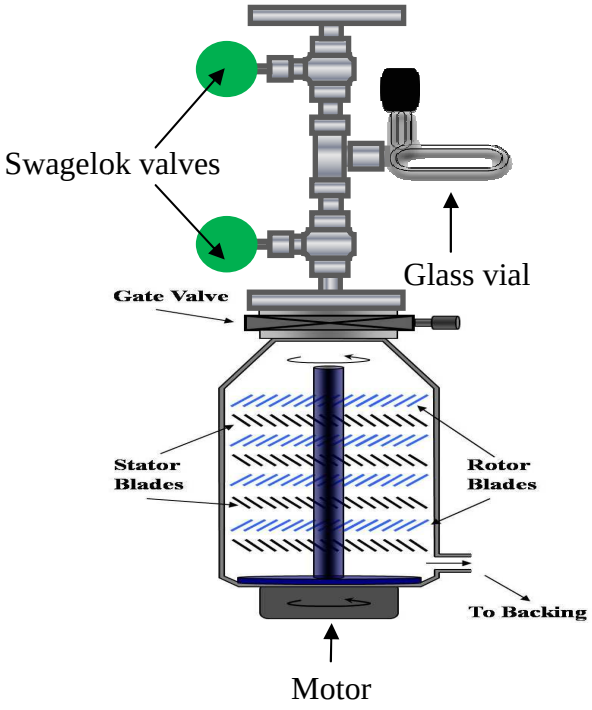

Figure 2.9. A diagram of a Knudsen source for dosing low-vapor pressure compounds.

2.4 Experimental Techniques

2.4.1 Temperature-Programmed Desorption (TPD)

Temperature-Programmed desorption (TPD) techniques are important methods for the determination of kinetic and thermodynamic parameters of desorption processes or decomposition reactions. A sample is heated with a temperature program and the partial pressures of atoms and molecules evolving from the sample are measured, by a mass spectrometer. When experiments are performed using well-defined surfaces of single-crystalline samples in a continuously pumped ultra-high vacuum (UHV) chamber then this experimental technique is often also referred to as thermal desorption spectroscopy (TDS). TPD is the technique that is most often used in this thesis.

In a TPD experiment, once reactant species are absorbed onto the surface of the sample, the temperature T of the sample is increased as a function of time t usually with a constant heating rate,

$$\beta(t) = dT/dt, \text{ so that:} \qquad (2.1)$$

$$T = T_0 + \beta t$$

As the temperature rises, the desorption rate of the species on the surface increases, lowering their coverage on the surface. These processes produce a peak in the partial pressure of the corresponding species as a function of temperature, (Figure 2.9). As TPD

experiment is being run, the partial pressure of the desorbing species is recorded with a mass spectrometer. The spectrum shows desorption of certain species as a function of temperature from which key information about the kinetics of the process can be obtained. The following points are worth noting

- The area under a peak is proportional to the amount originally adsorbed, i.e. proportional to the surface coverage.
- The kinetics of desorption (obtained from the peak profile and the coverage dependence of the desorption characteristics) give information on the state of aggregation of the adsorbed species e.g. molecular or dissociative adsorption.
- The position of the peak (the peak temperature) is related to the enthalpy of adsorption, i.e. to the strength of binding to the surface.
- By sequentially monitoring several masses, decomposition mechanisms and reaction products can be deduced.

The desorption rate r_{des} is normally expressed by a rate law of n^{th} order [6]:

$$r_{des} = -\frac{d\theta}{dt} = k_{des}\theta^n \qquad (2.2)$$

Where θ is the adsorbate species coverage and k_{des} the desorption rate constant. This activated process, k_{des} can be expressed by:

$$k_{des} = Aexp\left(-\frac{E_{des}}{RT}\right) \qquad (2.3)$$

Where A is a frequency factor, E_{des} the activation energy for desorption and R is the ideal gas constant. The Polanyi-Wigner equation (2.4) is formed from substituting in equation (2.3)

$$r_{des} = -\frac{d\theta}{dt} = A\theta^n exp\left(\frac{-E_{des}}{RT}\right) \tag{2.4}$$

as it pertains to the constant heating rate (Equation (2.1)), the rate of desorption as a function of temperature can be express as:

$$\frac{d\theta}{dT} = -\frac{1}{\beta} A\theta^n exp\left(\frac{-E_{des}}{RT}\right) \tag{2.5}$$

At the peak temperature T_p, the derivative of the data becomes zero and Equation (2.5) can be solved explicitly provided that E_{des} is independent of the coverage. Then:

$$\frac{E_{des}}{RT_p^2} = \frac{1}{\beta} A\theta^{n-1} exp\left(\frac{-E_{des}}{RT_p}\right) \tag{2.6}$$

In 1962, Redhead [7] derived a simple relationship between E_{des} and T_p by assuming that the activation parameters A and E_{des} where independent of the coverage, and also that the kinetics behave as first order. Solving Equation (2.6) for E_{des}, we obtain:

$$E_{des} = RT_p\left[ln\left(\frac{AT_p}{\beta}\right) - ln\left(\frac{E_{des}}{RT_p}\right)\right] \tag{2.7}$$

The Redhead method can be used to extract activation energies from a single TPD spectrum, if the frequency factor is available.

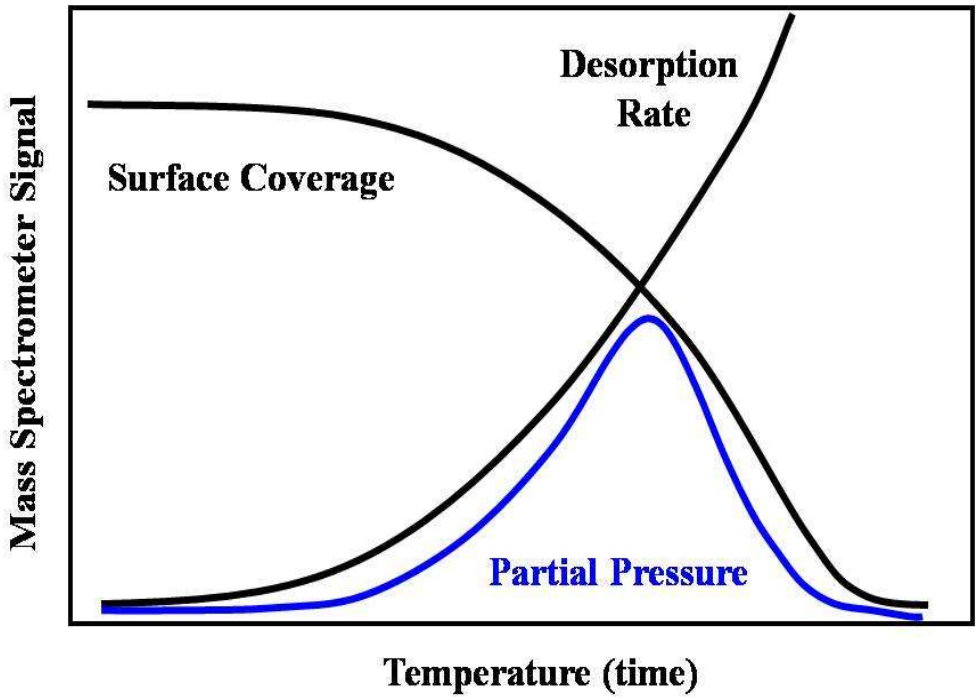

Figure 2.10. Illustrates the peak of partial pressure on TPD spectrum

2.4.2 Auger Electron Spectroscopy (AES)

Auger Electron Spectroscopy (Auger spectroscopy or AES) was developed in the late 1960's, based on the effect first observed by Pierre Auger, a French Physicist, in the mid-1920s [8]. AES is a surface - specific technique utilizing the emission of low energy electrons in the Auger process.

AES is one of the most generally employed surface analytical techniques for defining the composition of the surface layers of a sample. Auger spectroscopy can be considered as involving three elementary steps:

- Atomic ionization (by removal of a core electron)
- Electron emission (the Auger process)
- Analysis of the emitted Auger electrons

These steps are shown below in (Figure 2.10). First, an incident electron of energy, $E > E_{core}$, ionizes an atom by removing a core state electron (E_{core}). Second, the resulting vacancy is filled by an electron transition from a higher-energy shell (E_{L1}). Finally, the transition energy can be released either by emission of a photon, giving rise to X-ray fluorescence, or by energy transfer to a second, higher-energy shell electron (E_{L2}) called the Auger electron, which can be emitted from the atom with a kinetic energy E_K, and ∅ is the work function of the metal.

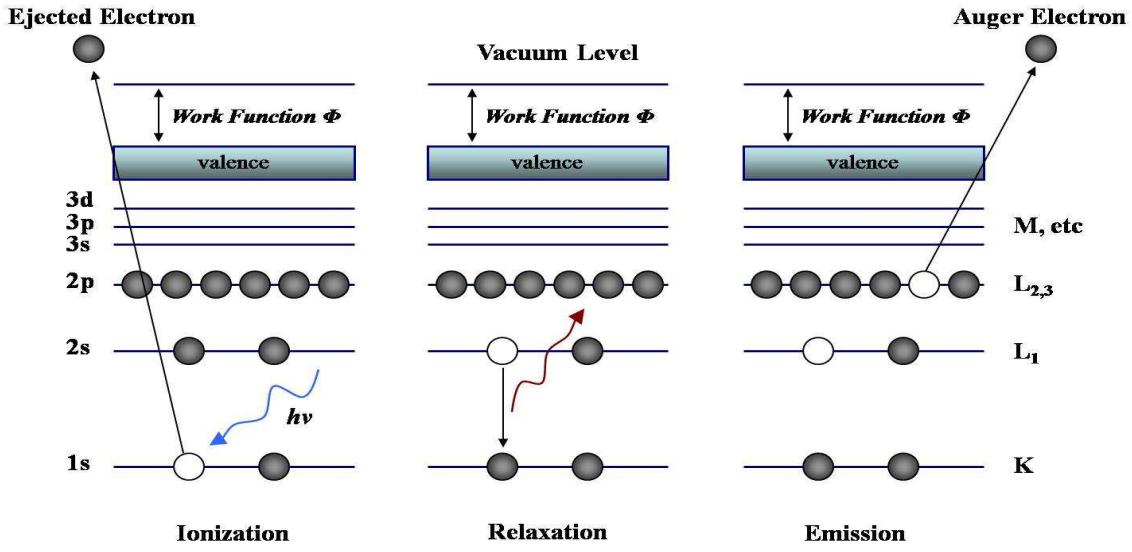

Figure 2.11. Auger energy process

The kinetic energy of the Auger electron can be written in equation:

$$E_K = E_{core} - E_{L1} - E_{L2} - \emptyset \qquad (2.8)$$

The Auger electron's kinetic energy E_K, depends on the binding energies of the electrons within the atom and not on the incident beam energy, thus this technique becomes sensitive to chemical composition by analyzing the distribution of the corresponding kinetic energies. Auger peaks are usually labeled with three letters corresponding to the energy levels from which the electrons involved originate.

2.4.3 Low Energy Electron Diffraction (LEED)

Low-energy electron diffraction (LEED) was first discovered experimentally by Clinton Davission and Lester Germer in 1927 [9]. During the last fifty years low energy electron diffraction (LEED) has provided a great deal of information on the structure of single crystal surfaces and of ordered atomic or molecular species on these surfaces. In recent years surface crystallography by LEED has effectively determined the detailed location of the atoms within the surface unit cell, and the bond lengths and orientations of ordered adsorbed molecules can be determined. LEED spot patterns represent the reciprocal lattice of the surface. The diffraction pattern must be inverted to real space in order to acquire the real-space periodicity [10]. An example of real space basis vectors *a*, *b* and reciprocal-space basis vectors *a*, *b* of a two-dimensional hexagonal lattice space is displayed in (Figure 2.93). Various changes can be monitored with LEED such as structural changes in surface coverage and also modifications by temperature at a given

coverage. The most commonly observed change is a disappearance of order when the temperature is increased. LEED is the principal technique for the determination of surface structures.

LEED may be used in one of two ways:

- Qualitatively: where the diffraction pattern is recorded and analysis of the spot positions yields information on the size, symmetry and rotational alignment of the adsorbate unit cell with respect to the substrate unit cell.
- Quantitatively: where the intensities of the various diffracted beams are recorded as a function of the incident electron beam energy to generate so-called I-Vcurves which, by comparison with theoretical curves, may provide accurate information on atomic positions.

The LEED technique uses a beam of electrons of a well-defined low energy (typically in the range 20 - 200 eV) incident normally on the sample. The sample itself must be a single crystal with a well-ordered surface structure in order to generate a back-scattered electron diffraction pattern. Only the elastically-scattered electrons contribute to the diffraction pattern; the lower-energy (secondary) electrons are removed by energy-filtering grids placed in front of the fluorescent screen that is engaged to display the pattern. The de Broglie relation is the wavelength of the electron:

$$\lambda = h/p \qquad (2.9)$$

where $p = \sqrt{2mE}$ is known as the momentum of the electron. The interference of electron waves diffracted by the periodic crystal lattice produces a diffraction pattern that can be related to the symmetry scattering of the scattered center. LEED is a surface

science technique that probes only the first few layers of the sample's surface. In this thesis the LEED technique was used on clean metals and AuPd alloys. Shown below (Figure 2.92). is face centered cubic unit cells for the (100) and (111) surfaces, which corresponds to the samples used in this thesis.

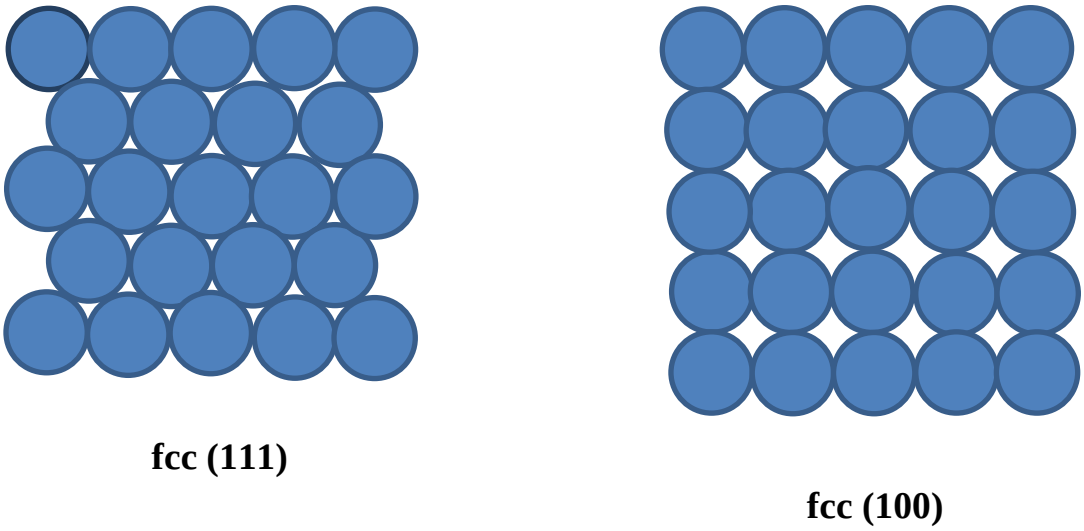

Figure 2.12. Fcc cubic unit cells

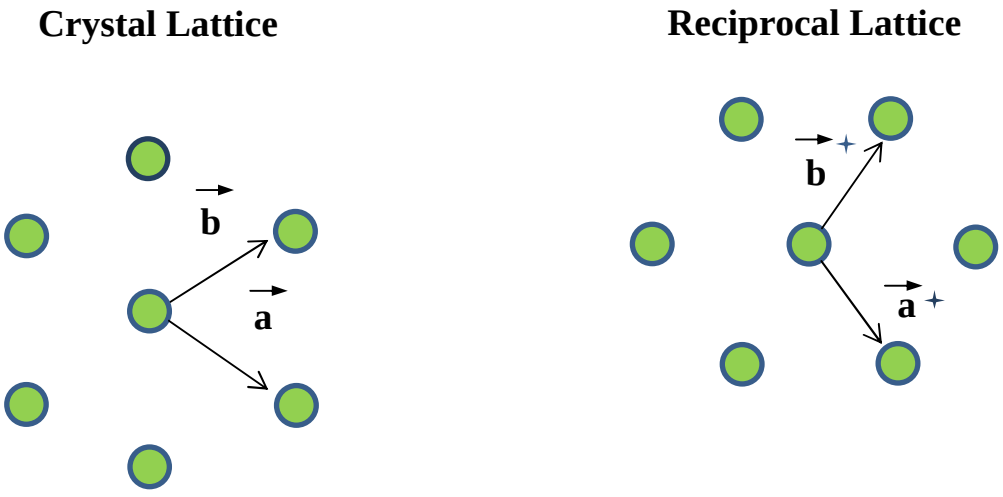

Figure 2.13. Real-space and reciprocal-space vectors (hexagonal lattice)

The chamber was configured with a four-grid, retarding-field analyzer with integral electron gun to collect LEED current/voltage (I/V) curves described in previous work [6-7]. The suppression box (retarding grids) was calibrated to 10v for the optimal output. The LEED photos were imaged using a Canon digital camera. Shown below in (Figure 2.13) is a schematic of electrons diffracting from the different faces of the crystal. Bragg's Law $n\lambda = 2d \sin\Theta$ is a key component in understanding the diffraction process, were n = order of diffraction as a integer 1, 2, 3…, λ = wavelength of incident wave, d = distance between atomic planes lattice, and Θ is angle between the incident ray and the scattering planes. Bragg's Law developed by the English physicists Sir W.H. Bragg and his son Sir W.L. Bragg in 1913 to explain why the cleavage faces of crystals appear to reflect X-ray beams at certain angles of incidence [8].

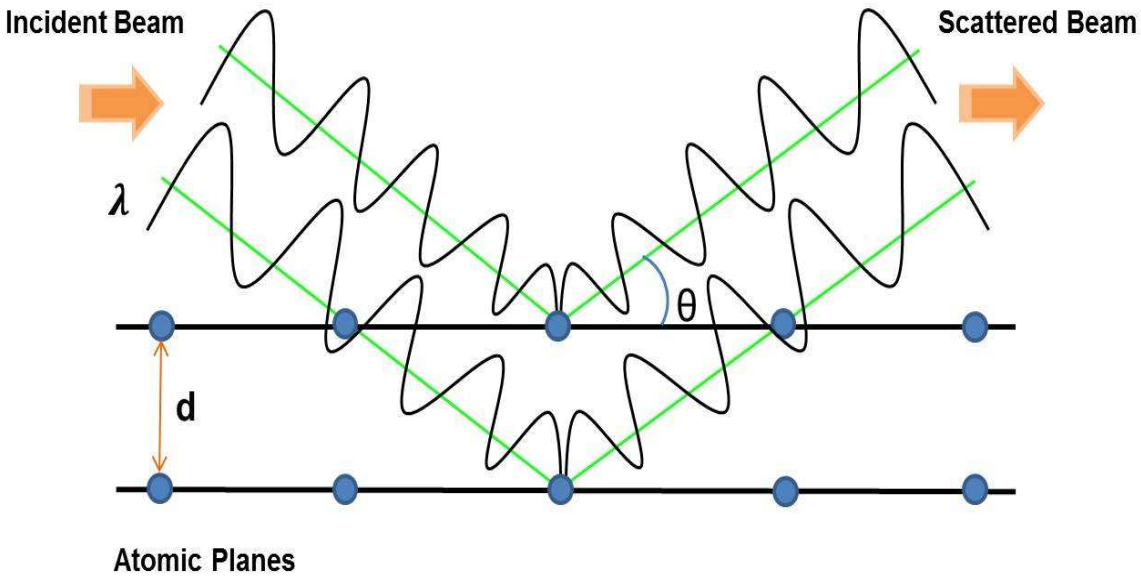

Figure 2.14. Bragg's Law: $n\lambda = 2d \sin\Theta$

The LEED experimental setup is shown in a schematic representation below (Figure 2.14). The process consist of an electron gun that produces an electron beam with a narrow kinetic energy range. This beam scatters from the sample surface through a set of charged grids which function to select only the electrons which elastically scatter from the surface, which are then accelerated to a fluorescent screen [11].

When they strike the screen, they cause the phosphor to glow, revealing a pattern of dots, which is the diffraction pattern. Here is a schematic representation of the equipment.

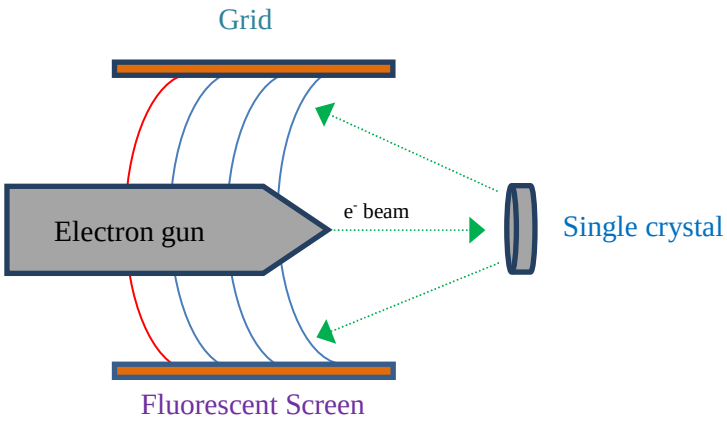

Figure 2.15. Low Energy Electron Diffraction equipment

2.4.4 Mass Spectrometer

The first application of mass spectrometry to the analysis of amino acids and peptides was reported in 1958 [12]. Mass spectroscopy is used to measure the characteristics of individual molecules; a mass spectrometer converts them to ions so that they can be

manipulated by external electric and magnetic fields. The three essential functions of a mass spectrometer, and the associated components, are:

- **Ion Source-** a small sample is ionized, usually to cations by loss of an electron.
- **Mass Analyzer**- the ions are sorted and separated according to their mass and charge.
- **Detector-** the separated ions are then measured and the results displayed on a chart.

Mass spectrometers are primarily used for residual gas analysis in the UHV chamber. They can also be used for leak detection and gas purity verification. During surface analysis and the study of reaction pathways, mass spectrometers are used for TPD experiments. The TPD chamber uses an Ametek Dycor quadrupole gas analyzer, which consists of four hyperbolic rods that D.C. and R.F. voltages are applied. Gas molecules are ionized by electrons from the filament.

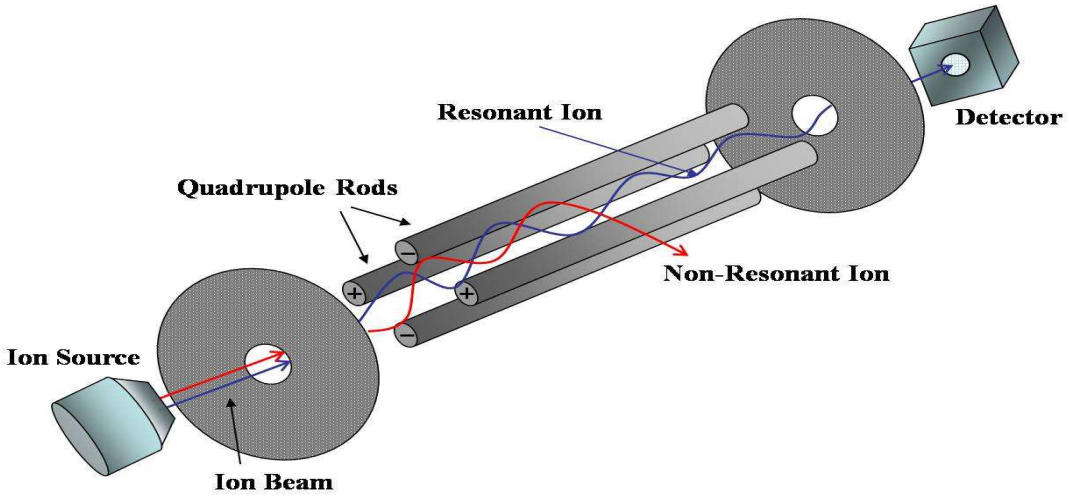

Figure 2.16. Quadrupole Mass Spectrometer analyzer

The positive ions formed are accelerated by the grids into the quadrupole section where they are separated by their mass. They are detected by the electron multiplier after exiting the aperture. A schematic diagram of a quadrupole mass spectrometer analyzer is presented in (Figure 2.95). For TPD experiments the mass spectrometer is operated in pressure vs. time mode. A specially designed LabView software program is used to automatically control the mass spectrometer and the TPD system. The program allows five different masses to be recorded sequentially while the temperature of the sample is synchronously recorded by a computer. This program allows for the modification of heating rates and temperature heating ranges. The data collected from the mass spectrometer is transferred into the Lab View program on a computer for analysis.

2.4.5 Ozone Generator

Ozone or (trioxygen) is a highly reactive form of oxygen; it is formed by the recombination of molecular and atomic oxygen. One of the oxygen atoms in an ozone molecule is weakly bonded which makes it highly unstable and yet very reactive. In the upper atmosphere ozone acts as a layer of protection that shields the earth from the harmful uv-rays, unfortunately at ground level ozone is a harmful pollutant.

There are various methods used for the adsorption of atomic oxygen onto gold surfaces, such as the electron-assisted activation, thermal dissociation of molecular oxygen over a hot filament, the reaction of preadsorbed H_2O and NO_2, exposure to an oxygen plasma, oxygen-sputtering and the exposure to ozone. The higher activity of ozone compared to molecular oxygen makes it possible to introduce oxygen in a vacuum chamber at low pressures. The ozone system used for the research presented in this thesis consists of an

oxygen cylinder connected to a Lab 5GA2Z ozone generator capable of producing 5g/hr of ozone. The ozone generator uses a fan-cooled Corona Discharge (CD) tube to generate ozone. The production of ozone can be controlled on both the input and output sides of the unit. The amount of air or oxygen entering is varied by an adjustable flow regulator, while the concentration of ozone discharged is varied by a potentiometer on the Corona Discharge tube. The ozone generated is transferred to the vacuum chamber through a Swagelok connection. The amount of ozone introduced into the vacuum chamber is controlled by a variable leak valve. All connections and tubing in direct contact with ozone were either Telfon or glass to minimize the decomposition of ozone. A glass direct dosing tube which was used to introduce ozone to the sample was conditioned with ozone for several hours before experiments. This method of adsorbing oxygen onto inert surfaces is very safe without the danger of explosions when trapping ozone; it's well controlled, clean and requires little to no maintenance.

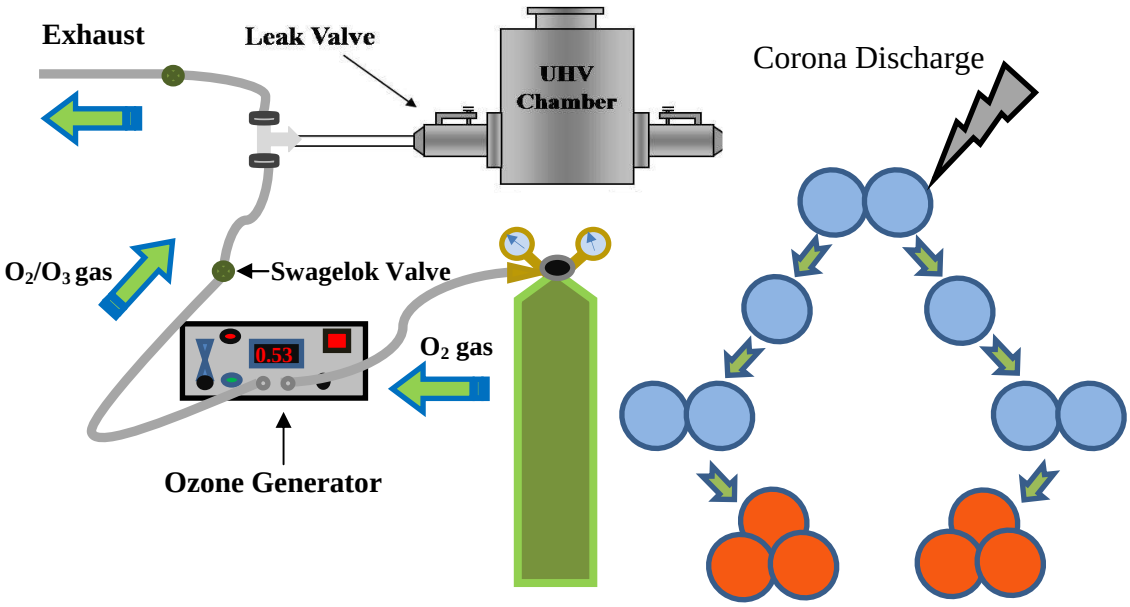

Figure 2.17. Ozone generator system and formation process

2.5 References

[1] Power, B.D. *High Vacuum Pumping Equipment,* Reinhold, New York, **1966**

[2] Gaede, W. *Annalen der Physik,* **1915**, *46, 357*

[3] Besancon R.M. *Vacuum Techniques (3rd ed.),* Van Nostrand Reinhold, New York, **1990**

[4] W.J. Wytenburg and R.M. Lambert, J. Vac. Sci. Technol. A, 10 **(1992),** 3597

[5] UKSAF.org /CMA **(2006)**

[6] O. Furlong, Ph.D thesis, University of Wisconsin-Milwaukee, **2010**

[7] Redhead, P.A. Vacuum, **1962**, 12, 203

[8] Auger, M.P. *Compt. Rend*., **1925**, 180

[9] C. Davisson, L.H. Germer. Nature 119 **(1927)** 558

[10] Sydney G. Davison, *Progress in Surface Science,* Vol. 23(2/3), **1986**

[11] D. Thomas University of Padova, Dept of Chemical Science. **(1995)**

[12] De Hoffmann, E.; Stroobant. V. Mass Spectrometry: Principles and Applications (2nd ed.), John Wiley & Sons, Ltd, Toronto, **2003**

Chapter 3: The Structure of Au/Pd(100) alloy surfaces characterized by Low-energy electron diffraction (LEED)

3.1 Introduction

The ability to produce ideal model catalysts is very important in the Surface science field. To enhance catalytic performance of these catalysts various strategies can be used in the preparation process. One approach in this quest is to produce an alloy surface that increases the activity of the surface. Au/Pd alloys which are used in this work can be created by depositing several amounts of gold onto the palladium substrate. To form different compositions the alloy is heated and annealed to various temperatures, which allows the gold to diffuse into the bulk [1-5]. Heating the substrate can form a wide-range of alloy surfaces that can be used in a single experiment. To understand the composition of the surface and how it affects the surface chemistry, it is important to know the coverage of the gold and palladium as a function of the mole fraction of the different elements present in the bulk of the sample. It is also important to focus on the distribution of the gold and palladium atoms on the surface. Gold can be expected to segregate to the surface due to it having a surface free energy of 1.63J/m^2 [6] which is lower than palladium that has a surface free energy of 2.05 J/m^2 [7]. In previous studies DFT and Monte Carlo simulations suggest that palladium and gold atoms are not randomly

distributed on the surface of the alloy [8-9]. These studies also propose that there is a net repulsive interaction between the gold atoms that is responsible for a larger collection of isolated atoms than would be expected from random distribution. These alloys are very stable due to the fact that gold is relatively inert to most contaminants, but the composition of the alloy can be altered by the presence of adsorbates [10].

To determine the coverage of the gold and palladium, Auger spectroscopy (AES) was used to probe the sample [1-5]. AES is surface sensitive but can only examine the first few layers of the surface, so only an average of the composition is determined. To understand to outermost layer of the alloy LEED is instilled. LEED not only aids in the determination of surface coverage, but also reveals structural changes and order of the surface. LEED is carried out with electron energies up to ~150 eV, which corresponds to the electron mean-free path is not far from its minimum value. The LEED images must be analyzed by measuring the different intensities produced versus beam energies of the diffraction spots of the alloy surface. The diffraction spots can assist in the determination of the alloy composition and can investigate not only the outmost layer but deeper layers by adjusting the electron beam energy. The fractional ordered spots can present evidence that an adsorbate is existent on the surface and the order of the surface.

3.2 Experimental Methods

The equipment used for collecting LEED patterns has been described previously in chapter 2 of this thesis [59]. LEED measurements were carried out in a μ-metal-shielded ultrahigh vacuum chamber operating at a base pressure of 5×10^{-11} Torr containing a Pd(100) single crystal, which could be cooled to 80 K and resistively heated to 1200 K.

The Pd(100) single crystal was cleaned using a standard procedure defined in chapter 2 of this thesis [60]. Gold was evaporated from a small alumina tube furnace [61] that allowed controlled and reproducible evaporation rates to be achieved. In order to control the source temperature, a C-type thermocouple was placed into the gold pellet. The amount of gold deposited onto the surface was monitored using Auger spectroscopy from the peak-to-peak intensities of the Au_{NVV} and Pd_{MNN} Auger features and the monolayer coverage was gauged from breaks in the gold uptake signal [55] which is shown in (Figure 3.3). The gold-palladium alloy was formed by initially depositing four monolayers of gold onto the Pd(100) substrate and then annealing to various temperatures for a period of five minutes in ultrahigh vacuum to produce the desired Au/Pd atomic ratio [55].

3.3 Results

The results of the DFT calculations presented studied along with this work [56] as well as experimental evidence show that no nearest-neighbor (palladium-palladium bridge) sites for gold coverages $\geq$0.5 ML [56] imply that the surface should exhibit order. This was explored by measuring the LEED patterns as a function of the composition of the Au/Pd(100) alloys. The Pd(100) substrate LEED pattern exhibits a (1×1) surface with no ordered structures found to be present on the clean surface. There were no initial additional ordered LEED patterns present for the unannealed 5 monolayer alloy surface, while probing the surface at eV energies from 55-260 eV, although there were 1^{st} and 2^{nd} order substrate patterns. Shown below are images of these patterns in (Figure 3.1). LEED patterns of Au/Pd(100) alloys for palladium coverages of 0.50, 0.76 and 0.87 ML are

revealed in (Figure 3.2). Shown also are the coverage ranges over which the c(2×2), (3×3) and (1×1) diffraction patterns appear.

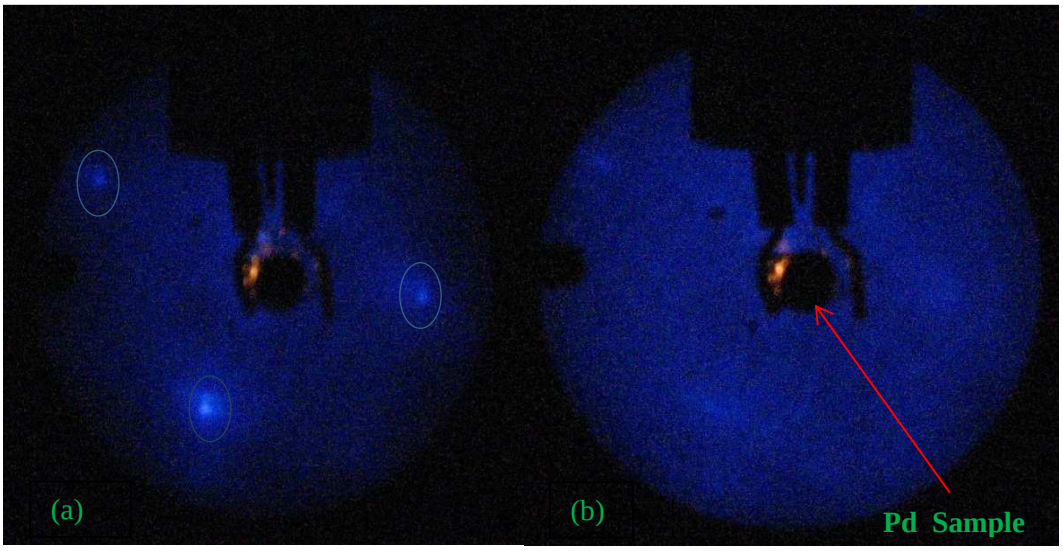

Figure 3.1. (a) LEED image of clean Pd(100) single crystal taken at ~70 eV **(b)** Unanneal Au/Pd(100) alloy with 5 monolayers of Au.

these additional spots which confirms a more weakly ordered surface. As the alloy composition is changed by increasing the annealing temperatures the surface becomes more ordered and sharper diffraction spots appear. With the formation of the AuPd(100) alloys, additional spots that appear due to ordered structures due to the presence of the gold atoms. The gold and palladium atoms are not randomly distributed on the surface. As each alloy is annealed Au atoms are mobilized and diffuse into the bulk.

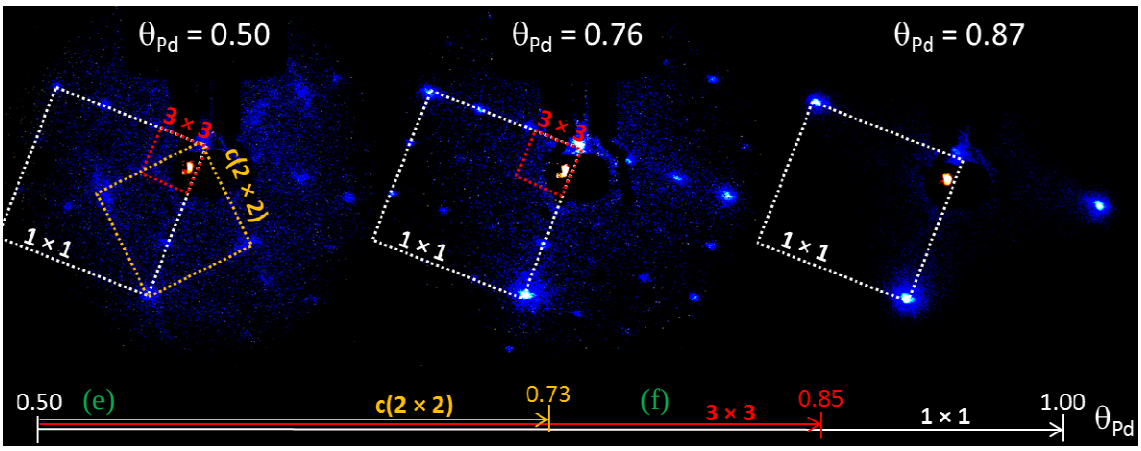

Figure 3.2. LEED patterns of Au/Pd(100) alloys for palladium coverages of 0.50, 0.76 and 0.87 ML. Shown also are the coverage ranges over which the c(2×2), (3×3) and (1×1) diffraction patterns appear.

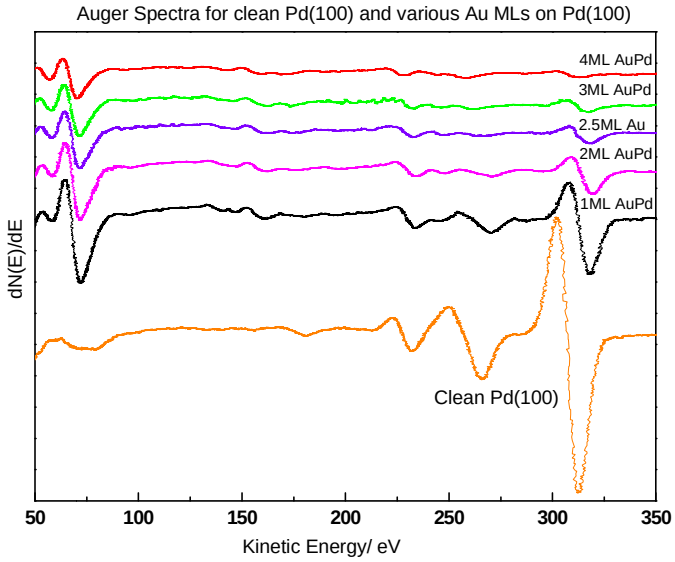

Figure 3.3. Auger Spectra showing clean Pd(100) surface and various coverages of gold evaporated on the Pd substrate.

3.4 Discussion

The LEED spot spacing versus alloy annealing temperatures shows the structure of the gold palladium surface of the alloy at various compositions. The range of interactions found on the (100) face of the model gold-palladium is distinctly different from that found on the (111) face. In the latter case both DFT calculations and the lack of any surface order by LEED indicated that only nearest-neighbor interactions were important [43-44], resulting in an almost random distribution of the surface gold and palladium atoms. In contrast LEED and DFT experiments Figure 2 confirm the existence of longer-range interactions on the (100) face.

3.5 Conclusion

The distribution of gold and palladium atoms in an Au/Pd(100) alloy was modeled using DFT and explored experimentally by LEED. Both the calculations and diffraction results revealed that there are longer-range interaction on Au/Pd(100) alloys than for Au/Pd(111). The LEED images show additional spots other than the substrate structure which corresponds to Au absorbate atoms on the palladium surface. With the heating of the alloy to above 1200 K the sample displayed similar patterns of a clean Pd(100) crystal, suggesting that most of the Au diffuses into the bulk.

3.6 References

[1] Gao, F.; Wang, Y.L. Goodman, D.W. *J. Am. Chem. Soc.* **2009,** *131*, 5734-5735.

[2] Gao, F.; Wang, Y.L. Goodman, D.W. *J. Phys. Chem. C* **2009,** *113*, 14993-15000.

[3] Piednoir, A.; Languille, M.A.; Piccolo, L.; Valcarcel, A.; Aires, F. J. C. S.; Bertolini, J-C. *Catal. Lett.* **2007**, *114*, 110-114.

[4] Baddeley, C.J.; Tikhov, M.; Hardacre, C.; Lomas, J.R.; Lambert, R.M. *J. Phys. Chem.* **1996**, *100*, 2189-2194.

[5] Baddeley, C.J.; Ormerod, R.M.; Stephenson, A.W.; Lambert, R.M. *J. Phys. Chem.* **1995**, *99* 5146-5151.

[6] U.S. Patent number 365888, 1967

[7] U.S. Patent number 08/670860, 1996

[8] Samanos, B.; Boutry, P.; Montarnal, R. *J. Catal.* **1971**, *23*, 19-30.

[9] Moiseev, F.L.; Vargaftik, M.N. In Perspectives in Catalysis, Chemistry for the 21st Century Thomas, J.M., Zhamoriov. A. Eds.; Blackwell Science, 1992, p 91.

[10] Stacchiola, D.; Calaza, F.; Burkholder, L.; Schwabacher, A.W.; Neurock, M.; Tysoe, W.T. *Angew. Chem.* **2005**, *44*, 4572-4574

[11] Stacchiola, D.; Calaza, F.; Burkholder, L.; Tysoe, W.T. *J. Am. Chem. Soc.* **2004**, *126*, 15384-15385.

[12] Gao, F.; Wang, Y.; Calaza, F.; Stacchiola, D.; Tysoe, W.T. *J. Mol. Catal.: A Chemical* **2008**, *281*, 14-23.

[13] Han, Y.F.; Kumar, D.; Sivadinarayana, C.; Clearfield, A.; Goodman, D.W. *Catal. Lett.* **2004**, *94*, 131-134.

[14] Chen, M.S.; Kumar, D.; Yi, C.W.; Goodman, D.W. *Science* **2005**, *310*, 291-293.

[15] Calaza, F.; Li, Z.; Gao, F.; Boscoboinik, J.; Tysoe, W.T. *Surf. Sci.* **2008**, *602*, 3523-3530.

[16] Chen, M.S.; Luo, K.; Wei, T.; Yan, Z.; Kumar, D.; Yi. C.W.; Goodman, D.W. *Catal. Today* **2006**, *117*, 37-45.

[17] Meenakshisundaram, S.; Nowicka, E.; Miedziak, P.J.; Brett, P.J. Jenkins, R.L.; Dimitratos, N.; Taylor, S.H.; Knight, D.W.; Bethell, D.; Hutchings, G.J. *Faraday Disc.* **2010**, *145*, 341-356.

[18] Lee, A.F.; Hackett, S.F.J.; Hutchings, G.J.; Lizzit, S.; Naughton, J.; Wilson, K. *Catal. Today* **2009**, *145*, 251-257.

[19] Dimitratos, N.; Lopez-Sanchez, J.A.; Morgan, D.; Carley, A.F.; Tiruvalam, R.; Kiely, C.J.; Bethell, D.; Hutchings, G.J. *Phys. Chem. Chem. Phys.* **2009**, *11*, 5142-5153.

[20] Li, G.; Enache, D.I.; Edwards, J.; Carley, A.F.; Knight, D.W.; Hutchings, G.J. *Catal. Lett.* 2006, 110, 7-13.

[21] Enache, D.I.; Edwards, J.K.; Landon, P.; Solsona-Espriu, B.; Carley, A.F; Herzing, A.A.; Watanabe, M.; Kiely, C.J.; Knight D.W.; Hutchings, G.J. *Science* **2006**, *311*, 362-264.

[22] Marx, S.; Baiker, A. *J. Phys. Chem. C* **2009**, *113*, 6191-6201.

[23] Landon, P.; Collier, P. J.; Papworth, A. J.; Kiely. C. J.; Hutchings, G.J. *Chem. Commun.* **2002**, 2058-2059.

[24] Edwards, J. K.; Solsona, B.E.; Landon, P.; Carley, A.F.; Herzing, A.; Kiely. C.J.; Hutchings, G.J. *J. Catal.* **2005**, *236*, 69-79.

[25] Pritchard, J.C.; He, Q.; Ntainjua, E.N.; Piccinini, M.; Edwards, J.K.; Herzing, A.A.; Carley, A.F.; Moulijn, J.A.; Kiely, C.J.; Hutchings, G.J. *Green Chem.* **2010**, *12*, 915-921.

[26] Piccinini, M.; Ntainjua, E.; Edwards, J.K.; Carley, A.F.; Moulijn, J.A.; Hutchings, G.J. *Phys. Chem. Chem. Phys.* **2010**, *12*, 2488-2492.

[27] Ntainjua, E.; Piccinini, M.; Pritchard, J.C.; He, Q.; Edwards, J.K.; Carley, A.F.; Moulijn, J.A.; Kiely, C.J.; Hutchings, G.J. *Chem.Cat.Chem.* **2009**, *1*, 479-484.

[28] Edwards, J.K.; Ntainjua, E.; Carley, A.F.; Herzing, A.A.; Kiely, C.J.; Hutchings, G.J. *Angew. Chem. Int. Ed.*, **2009**, *48*, 8512-8515.

[29] Edwin, N.N.; Piccinini, M.; Pritchard, J.C.; Edwards, J.K.; Carley, A.F.; Moulijn, J.A; Hutchings, G.J. *ChemSusChem.* **2009**, *2*, 575-580.

[30] Edwards, J.K.; Solsona, B.E.; N, E.N.; Carley, A.F.; Herzing, A.A.; Kiely, C.J.; Hutchings, G.J. *Science* **2009**, *323*, 1037-1041

[31] Edwards, J.K.; Hutchings, G.J. *Angew. Chem. Int. Ed.* **2008**, *47*, 9192-9198.

[32] Edwards, J.K.; Thomas, A.; Solsona, B.E.; Landon, P.; Carley, A.F.; Hutchings, G.J. *Catal. Today*. **2007**, *122*, 397-402.

[33] Edwards, J.K.; Carley, A.F.; Herzing, A.A.; Kiely, C.J; Hutchings, G. *Farad, Disc.* **2008**, *138*, 225-239.

[34] Solsona, B.E.; Edwards, J.K.; Landon, P.; Carley, A.F.; Herzing, A.; Kiely, C.J.; Hutchings, G.J. *Chem. Mater*. **2006**, *18*, 2689-2695.

[35] Edwards, J.K.; Solsona, B.; Landon, P.; Carley, A.F; Herzing, Watanabe, M.; Kiely, C.J.; Hutchings, G.J. *J. Mater. Chem.* **2005**, *15*, 4595-4600.

[36] Edwards, J.K.; Solsona, B.E.; Landon, P.; Carley, A.F.; Herzing, A.; Kiely, C.J.; Hutchings, G.J. *J. Catal.* **2005**, *236*, 69-79.

[37] Landon, P.; Collier, P.J.; Carley, A.F.; Chadwick, D.; Papworth, A.J.; Burrows, A.; Kiely, C.J.; Hutchings, G.J. *Phys. Chem. Chem. Phys.* **2003**, *5*, 1917-1923.

[38] Han, P.; Axnanda, S.; Lyubinetsky, I.; Goodman, D.W. *J. Am. Chem. Soc.* **2007**, *129*, 14355-14361.

[39] Baddeley, C.J.; Tikhov, M.; Hardacre, C.; Lomas, J.R.; Lambert, R.M. *J. Phys. Chem.* **1996**, *100*, 2189-2194.

[40] Ham, H.C..; Hwang, G.S.; Han, J.; Nam, S.W.; Lim, T.H. *J. Phys. Chem. C* **2009**, *113*, 12943-12945.

[41] Joshi, A.M.; Delgass, W.N.; Thomson, K.T. *J. Phys. Chem. C* **2007**, *111*, 7384-7395.

[42] Boscoboinik, J.A.; Plaisance, C.; Neurock, M.; Tysoe, W.T. *Phys. Rev. B* **2008**, *77*, 045422

[43] Li, Z,; Furlong, O.; Calaza, F.; Burkholder, L.; Poon, H.C; Saldin, D.; Tysoe, W.T. *Surf. Sci.* **2008**, *602*, 1084-1091.

[44] Boscoboinik, J.A.; Calaza, F.C.; Garvey, M.T.; Tysoe, W.T. *J. Phys. Chem. C.* **2010**, *114*, 1875-1880.

[45] Hoffmann, F.M. *Surf. Sci. Rep.* **1983**, *3*, 107-192.

[46] Kuhn, W.K.; Szanyi, J.; Goodman, D.W. *Surf. Sci. Lett.* **1992**, *274*, L611-L618.

[47] Szanyi, J.; Kuhn, W.K.; Goodman, D.W. *J. Vac. Sci. Technol.* **1993**, *A11*, 1969-1974.

[48] Ruggiero, C.; Hollins, P. *J. Chem. Soc., Faraday Trans.* **1996**, *92*, 4829-4834.

[49] Jugnet, Y.; Cadete Santos Aires, F.J.; Deranlot, C.; Piccolo, L.; Bertolini, J.C. *Surf. Sci.* **2002**, *521*, L639-L644.

[50] Meier, D.C.; Bukhtiyarov, V.; Goodman, D.W. *J. Phys. Chem. B* **2003**, *107*, 12668-12671.

[51] Ozensoy, E.; Goodman, D.W. *Phys. Chem. Chem. Phys.* **2004**, *6*, 3765-3778.

[52] Yi, C.W.; Luo, K.; Wei, T.; Goodman, D.W. *J. Phys. Chem. B* **2005**, *109*, 18535-18540.

[53] Wei, T.; Wang, J.; Goodman, D.W. *J. Phys. Chem. C* **2007**, *111*, 8781-8788.

[54] Li, Z.; Gao, F.; Wang, Y.; Burkholder, L.; Tysoe, W.T. *Surf. Sci.* **2007**, *601*, 1898-1908.

[55] Li, Z.; Gao, F.; Tysoe, W.T. *J. Phys. Chem. C* **2010**, *114*, 16909-16916.

[56] Behm, R.J.; Christman, K.; Ertl, G.; Van Hove, M.A. *J. Chem. Phys.* **1980**, *73*, 2984-2995.

[57] Tracy, J.C.; Palmberg, P.W. *J. Chem. Phys.* **1969**, *51*, 4852-4862.

[58] Zheng, T.; Stacchiola, D.; Poon, H. C.; Saldin, D. K.; Tysoe, W.T. *Surf. Sci.* **2004**, *564*, 71-78.

[59] Li, Z.; Gao, F.; Tysoe, W.T. *Surf. Sci.* **2008**, *602*, 416-423.

[60] Wytenburg, W.J.; Lambert, R.M. *J. Vac. Sci. Technol.* **1992**, *A10*, 3597-3598.

[61] Kresse, G.; Joubert, J. J. *Phys. Rev. B* **1999**, *59*, 1758-1775.

[62] Blöchl, P.E. *Phys. Rev. B* **1994**, *50*, 17953-17979.

[63] Kresse, G.; Hafner, J. *Phys. Rev. B* **1993**, *47*, RC558-RC561.

[64] Kresse, G.; Furthmüller, J. *Phys. Rev. B* **1996**, *54*, 11169-11186.

[65] Kresse, G.; Furthmüller, *J. Comput. Mat. Sci*. **1996**, *6*, 15-50.

[66] Perdew, J.P.; Burke, K.; Ernzerhof, M. *Phys. Rev. Lett.* **1996**, *77*, 3865-3868.

[67] Kawasaki, K. *Phys. Rev.* **1966**, *145*, 224-230.

[68] Sayle, R.; Milner-White, E.J. *Trends in Biochemical Sciences (TIBS)*, **1995**, *20*, 374-376.

[69] Pendry, J. B. Low Energy Electron Diffraction (Academic Press, London, 1974)

Chapter 4: Adsorption of 1,3-Phenylene Diisocyanide on Au(111)

4.1 Introduction

It has been shown previously that 1,4-phenlyene diisocyanobenzene (1,4-PDI) on Au(111) react to form one-dimensional oligomer chains comprising alternating gold and 1,4-PDI units on the Au(111) surface [1-3] This forms by extracting gold atoms from low-coordination sites on the gold surface. Since 1,4-PDI maintains its π-conjugation throughout the molecule and has two functional groups it has been proposed as a prototypical molecule for nanoelectronic applications [4-9]. It has also been recently demonstrated that it is possible to link between gold nanoparticles using a similar chemistry in which the 1,4-PDI extracts gold atoms from the golf nanoparticles to form an oligomeric bridge between them. In the case of 1,4-PDI, the spacing between the gold atoms in the –(Au-1,4-PDI)- repeat unit is close to four times the gold-gold nearest-neighbor distance along the close packed $< 1\bar{1}0 >$ directions on Au(111). However, DFT calculations suggest that there is some strain that distorts the plane of the 1,4-PDI molecule. [1] In order to explore whether the oligomerization found for 1,4-PDI is a general phenomenon and to ultimately explore the effect of molecular geometry on electron transport, the following explores the surface chemistry of 1,3-PDI on Au(111) surfaces using a range of surface-sensitive techniques.

4.2 Experimental

A Au(111) single crystal (Princeton Scientific) was cleaned with cycles of ion bombardment using 1 keV argon ions for 30 minutes (1 $\mu A/cm^2$), annealing to 900 K for 5 minutes and then to 600 K for 30 minutes. The sample could be cooled to 80 K in both chambers by thermal contact to a liquid-nitrogen-filled reservoir and resistively heated to ~1200 K. Reflection-absorption infrared spectroscopy (RAIRS) data were collected with a Bruker Equinox spectrometer, typically for 1000 scans at a resolution of 4 cm^{-1}. 1,4-phenylene diisocyanide (PDI) was obtained commercially (Aldrich Chemicals, 99% purity) and dosed via a home-built source as described previously.[2]

Density functional theory calculations were performed with the projector augmented wave (PAW) method[10,11] as implemented in the Vienna *ab initio* simulation package, VASP.[12-14] The exchange-correlation potential was described using the generalized gradient approximation (GGA) of Perdew, Burke and Ernzerhof.[15] A cutoff of 400 eV was used for the planewave basis set, and the wavefunctions and electron density were converged to within 1×10^{-5} eV. The first Brillouin zone was sampled with a 4×4×1 Γ-centered k-point mesh. Geometric relaxations were considered to be converged when the force was less than 0.02 eV/Å on all unrestricted atoms.

4.3 Results

The uptake and removal of 1,3-PDI on Au(111) at 300 K, monitored using Auger spectroscopy, is shown in (Figure 1). The initial uptake is shown in the top spectra where the growth of a feature at ~270 eV is due to the carbon KLL feature. This is mirrored by

the growth of a much less intense feature at ~380 eV due nitrogen (assigned to the N KLL signal). This indicates that both carbon and nitrogen adsorbs onto the surface, and is accompanied by a decrease in intensity of the gold signal (at ~70 eV) due to the low mean-free path of electrons at this kinetic energy. The variation in C KCL Auger signal with 1,3-PDI exposure is shown in (Figure 4.2). showing a smooth uptake of 1,3-PDI with increasing exposure. However, C KLL and N KLL signals show very little variation in intensity as the sample is heated to ~900 K indicating that the majority of the adsorbed 1,3-PDI is very stably adsorbed on the surface.

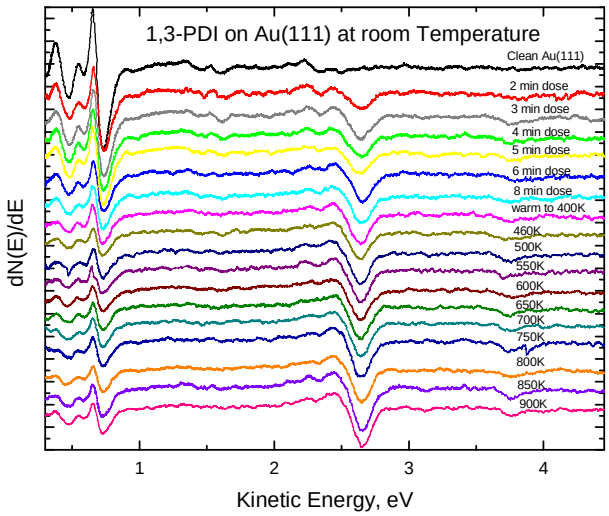

Figure 4.1. A series of Auger spectra after dosing 1,3-PDI on Au(111) at 300 K for up to 8 minutes and the effect of subsequent heating to 900 K.

The corresponding temperature-programmed desorption (TPD) profiles are shown in Fig 4.3(a) shows the 76 amu profiles and profiles collected at 26, 50 and 64 amu show identical shapes. Comparison of the relative intensities of the features with the mass spectrometer ionizer fragmentation pattern of 1,3-PDI confirms that the feature is due to the desorption of molecular 1,3-PDI. The spectra consist of a sharp feature centered at

~225 K at low exposures that shifts slightly to higher temperatures (~230 K) as the 1.3-PDI exposure increases.

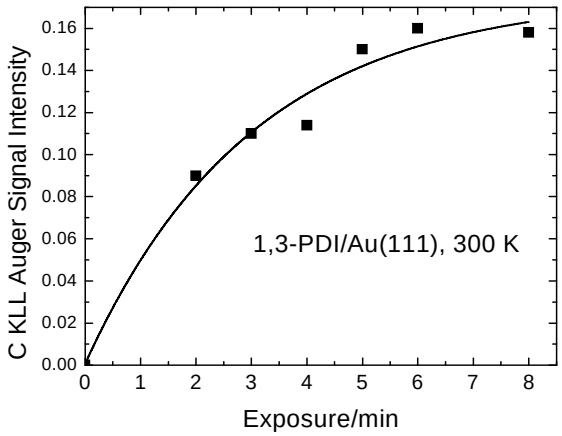

Figure 4.2. Uptake of 1,3-PDI on Au(111) at 300 K from the peak-to-peak intensity of the carbon KLL Auger features in the spectra shown in (Fig. 4.1)

The intensities of the signals after 2 and 4 minutes exposure are very similar indicating that this is not due to the desorption of 1,3-PDI multilayers and is ascribed to a small amount of 1,3-PDI adsorbed in the second layer. This is close to the desorption temperature of 1,4-PDI on Au(111) of ~245 K.[3] This assignment is confirmed by the observation that this sharp feature is absent at the lowest PDI exposure. This sharp feature is accompanied by a broad tail to higher temperatures. However, hydrogen is the only other species found to desorb from the surface (Figure 4.3(b)) which evolves in a broad feature centered at ~700 K. Thus, 1,3-PDI adsorbs very strongly on the Au(111) surface and is stable to above ~600 K, where it decomposes to evolve hydrogen (Figure 4.2(b)) and leave carbon and nitrogen on the surface (Figure 4.1) A small amount of additional 1,3-PDI adsorbs into the second layer to desorb at ~230 K (Fig. 4.3(a)).

(Figure 4.4) shows an STM image of 1,3-PDI dosed onto a Au(111) surface at 300 K and imaged a 120 K to minimize thermal effects. This clearly shows a zig-zag motif that might be expected of a bent molecule. In some cases, the patterns close in on themselves to form hexagonal units. There are brighter spots in some regions of the images, which may be associated with 1,3-PDI adsorbing into a second layer.

(a)

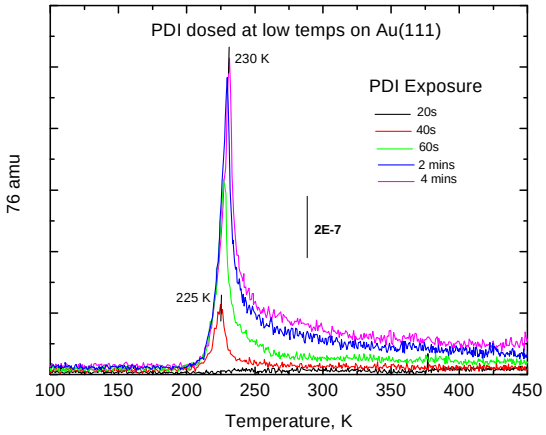

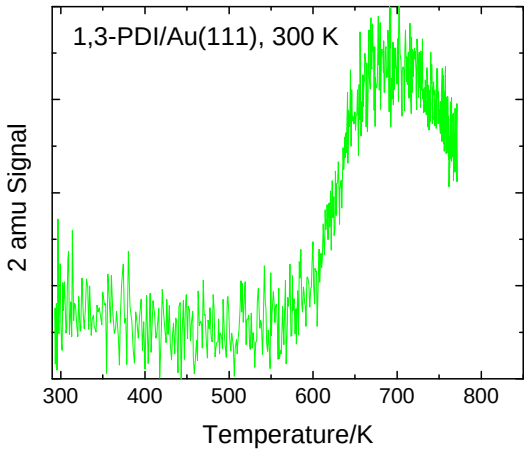

(b)

Figure 4.3. (a) TPD profiles for 1,3-PDI on Au(111) at 90 K as a function of exposure monitoring the 76 amu signal and (b) the 2 amu (hydrogen) desorption profile of a saturated overlayer to 1,3-PDI adsorbed at 300 K.

Finally, density functional theory calculations were performed to establish possible geometries of 1,3-PDI on the surface. Based on the structure found for 1,4-PDI, a structure was generated with gold adatoms on the Au(111) surface and the initial structures were set with the plane of 1,3-PDI set at various angles (30, 60 and 90°) with respect to the surface and the geometries allowed to relax. The most stable structure is depicted in (Figure 4.6), where the plane is tilted at ~30° to the surface with a binding energy of ~220 kJ/mol and is much larger than the energies of 1,3-PDI bonded directly to the gold surface (~60 kJ/mol).

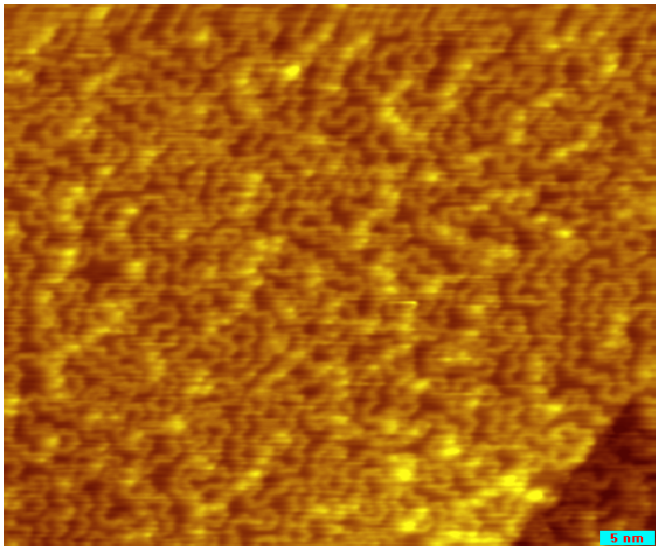

Figure 4.4 An STM image of a saturated overlayer of 1,3-PDI adsorbed on Au(111) at 300 K I_t= 98.pA, V_b= -1.0 V.

The large energy difference accounts for the 1,3- and 1,4-PDI being able to extract gold atoms from the substrate to form the oligomer chains. However, the energy to tilt the plane is rather small varying by only ~16 kJ/mol as the angle changes from perpendicular to the most stable structure (Figure 4.5).

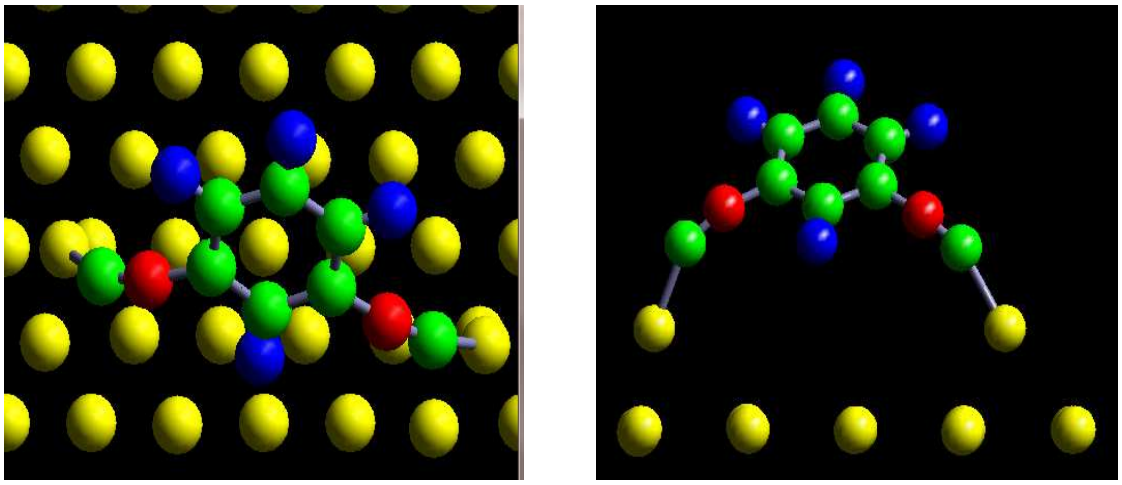

Figure 4.5. A depiction of the top and side views of 1,3-PDI adsorbed on gold adatoms on a Au(111) substrate calculated using density functional theory.

5.5 Discussion

1,3-PDI adsorbs strongly on Au(111) at 300 K and thermally decomposes to evolve hydrogen at ~700 K (Figure 4.4(b)) and leave carbon and nitrogen on the surface (Figure 4.1). Adsorption at ~90 K (Figure 4.3(a) results in 1.3-PDI desorption at ~230 K, close to the desorption temperature of 1,4-PDI from the surface.[3] This indicates that the chemistry of 1,3-PDI on Au(111) is similar to that found for 1,4-PDI, [1-4] which forms one-dimensional oligomer chains on the surface comprising repeat –(Au-PDI)- unites by extracting gold atoms from low-coordination sites on the Au(111) substrate. The TPD data (Fig. 4.3(b)) suggest that they are stable up to ~600 K, where they decompose by dehydrogenation leaving carbon and nitrogen on the surface (Figure 4.1). The low-temperature (~230 K) desorption state is due to 1,3-PDI bonded to the surface by a single isocyanide group and may be due to a precursor to the one-dimensional chain or to 1,3-PDI adsorbed on top of a saturated layer of the oligomer chain. This assignment is

supported by the observation that no 1,3-PDI desorbs from the surface at the lowest exposures since the initial 1,3-PDI oligomerizes on the surface.

The formation of stable species following 1,3-PDI adsorption is explored using density functional theory where the most stable adsorption geometry for a single 1,3-PDI molecule is shown in (Fig. 4.6). The stability of this species (~220 kJ/mol binding energy) is in accord with its stability found on heating (Figure 4.1(a) and 4.3(b)). The calculations suggest that the most stable structure has a molecular plane is tilted at ~30° to the surface. It should be noted, however, that calculations for 1,4-PDI bonding to gold suggest that there is a strong preference for the isocyanide groups to bond to gold adatoms in a trans geometry. [2] This would suggest that the oligomer chains formed from 1,3-PDI should have a tendency to form zig-zag structures with the plane of the molecule close to parallel to the surface to accommodate this trans geometry. This conjecture is borne out by the STM images of 1,3-PDI on Au(111) (Figure. 4.4), where a lathe number of such structures are identified. However, there are clearly also regions in which this zig-zag structure is not maintained and in several cases, hexagonal structures can be discerned. This is likely to be a result of steric constraints that prevent the zig-zag chains from forming. There are a number of brighter regions that may arise from 1,3-PDI adsorbed into a second layer on top of the oligomer chains.

5.6 Conclusions

The adsorption of 1,3-PDI on Au(111) at 300 K forms predominantly zig-zag chains on the surface consistent with the structures found previously for 1,4-PDI on Au(111). Structures are therefore proposed to bind to gold atoms extracted from defect sites on the surface. However, other motifs are also observed, for example hexagonal units that are proposed to form due to spatial constraints on the surface. The proposed

surface structure is consistent with the infrared spectra, which shows the presence of a single isocyanide mode and out-of-plane C-H modes that are consistent with the presence of molecular 1,3-PDI on the surface. The intensities of the infrared modes decrease a higher coverages and this effect can be ascribed to either a change in orientation as the polymer chains grow and to the change in symmetry between the isolated molecule and the factor group of the oligomer. The chains are extremely stable on the surface and thermally decompose only on heating above 600 K. A low-temperature (~230 K) desorption state is detected when 1,3-PDI is adsorbed at ~90 K, due either to 1,3-PDI bonded to the gold surface via a single isocyanide group or bonded to gold atoms in the oligomer chain.

5.7 References

[1] Boscoboinik, J.; Kestell, J.; Garvey, M.; Weinert, M.; Tysoe, W. *Top. Catal.* **2011**, *54*, 20.

[2] Boscoboinik, J. A.; Calaza, F. C.; Habeeb, Z.; Bennett, D. W.; Stacchiola, D. J.; Purino, M. A.; Tysoe, W. T. *Physical Chemistry Chemical Physics* **2010**, *12*, 11624.

[3] Zhou, J.; Acharya, D.; Camillone, N.; Sutter, P.; White, M. G. *The Journal of Physical Chemistry C* **2011**, *115*, 21151.

[4] Ito, M.; Noguchi, H.; Ikeda, K.; Uosaki, K. *Phys. Chem. Chem. Phys.* **2010**, *12*, 3156.

[5] Kim; Beebe, J. M.; Jun, Y.; Zhu, X. Y.; Frisbie, C. D. *Journal of the American Chemical Society* **2006**, *128*, 4970.

[6] Li, Y.; Lu, D.; Swanson, S. A.; Scott, J. C.; Galli, G. *The Journal of Physical Chemistry C* **2008**, *112*, 6413.

[7] Murphy, K. L.; Tysoe, W. T.; Bennett, D. W. *Langmuir* **2004**, *20*, 1732.

[8] Robertson, M. J.; Angelici, R. J. *Langmuir* **1994**, *10*, 1488.

[9] Shih, K.-C.; Angelici, R. J. *Langmuir* **1995**, *11*, 2539.

[10] Kresse, G.; Joubert, D. *Phys. Rev. B* **1999**, *59*, 1758.

[11] Blöchl, P. E. *Phys. Rev. B* **1994**, *50*, 17953.

[12] Kresse, G.; Hafner, J. *Phys. Rev. B* **1993**, *47*, 558.

[13] Kresse, G.; Furthmüller, J. *Phys. Rev. B* **1996**, *54*, 11169.

[14] Kresse, G.; Furthmüller, J. *Computational Materials Science* **1996**, *6*, 15.

[15] Perdew, J. P.; Burke, K.; Ernzerhof, M. *Phys. Rev. Lett.* **1996**, *77*, 3865.

[16] Henderson, J. I.; Feng, S.; Bein, T.; Kubiak, C. P. *Langmuir* **2000**, *16*, 6183.

[17] Swanson, S. A.; McClain, R.; Lovejoy, K. S.; Alamdari, N. B.; Hamilton, J. S.; Scott, J. C. *Langmuir* **2005**, *21*, 5034.

[18] Han, H. S.; Han, S. W.; Joo, S. W.; Kim, K. *Langmuir* **1999**, *15*, 6868.

[19] Colthup, N. B.; Daly, L. H.; Wiberley, S. E. *Introduction to infrared and raman spectroscopy. 2.ed*; Academic Press: New York,N.Y., 1975.

[20] Greenler, R. G. *The Journal of Chemical Physics* **1966**, *44*, 310.

[21] Greenler, R. G. *The Journal of Chemical Physics* **1969**, *50*, 1963.

[22] Liang, C. Y. *Journal of Molecular Spectroscopy* **1957**, *1*, 61.

[23] Tobin, M. C. *The Journal of Chemical Physics* **1955**, *23*, 891.

Chapter 5: LEED Characterization of Cu foil

5.1 *Introduction*

Sulfur-containing molecules, in particular those with sulfur-sulfur linkages, are used as lubricant additives for ferrous surfaces[1-14] so that dialkyl disulfides have been used as simple model compounds to explore the surface and tribological chemistry on iron [15,16] where they react at the high temperatures attained at the interface during rubbing to deposit a ferrous sulfide film. However, the tribological chemistry can depend critically on the nature of the substrate so that a good lubricant additive for one type of surface may not be applicable to another. In particular, the lubrication of sliding copper-copper interfaces in electrical motors[17-20] provides a particular challenge. Gas-phase lubricants based on water vapor have been used to reduce friction and wear,[21-25] but they tend to lead to asymmetric wear rates and failure at higher temperatures[26-27]. The following explores the chemistry of dimethyl disulfide (DMDS) on copper surfaces to establish whether it is sufficiently reactive to potentially form a tribofilm near room temperature as required for lubrication of the sliding copper-copper contact in an electric motor. These experiments will provide the background information for ultimately examining the frictional properties of dialkyl disulfides in ultrahigh vacuum (UHV)[28-32]and are thus carried out on both a Cu(111) single crystal substrate and copper foils, since the latter type of sample will eventually be examined in the UHV tribometer rather than single crystal samples.

5.2 *Experimental Methods*

Low-energy electron diffraction (LEED) experiments were carried out in a chamber operating at a base pressure of 8 x 10-11Torr.The sample in this chamber could be cooled to 80Kby contact with a liquid-nitrogen-filled reservoir and resistively heated to 1000 K.The copper foil samples were polished to a mirror finish using 1 μm diamond paste in a random orbit polisher. Once in UHV, the Cu(111) single crystal and copper foils were cleaned using a standard procedure which consisted of argon ion bombardment (~1 kV, ~ 2 μA/cm2) and annealing cycles up to ~850 K, and the cleanliness of the samples was monitored using Auger spectroscopy.

5.3 *Results*

The surface chemistry of DMDS ($(CH_3S)_2$) was studied on copper samples consisting of a polished, high-purity copper foil and a Cu(111) single crystal, both of which had been cleaned in UHV using the procedures indicated above. Initial LEED experiments were performed on a polished copper foil that had been cleaned by argon ion bombardment and heating. After several repetitions of this cleaning procedure, a faint, square (1 x 1) LEED pattern was found at 187 eV electron beam energy. After repeating the cleaning/annealing cycle four more times, the square (1 x 1) LEED pattern became significantly sharper and was visible over a wide range of electron beam energies from 70 to 235 eV which is shown in (Figure 5.1) below.

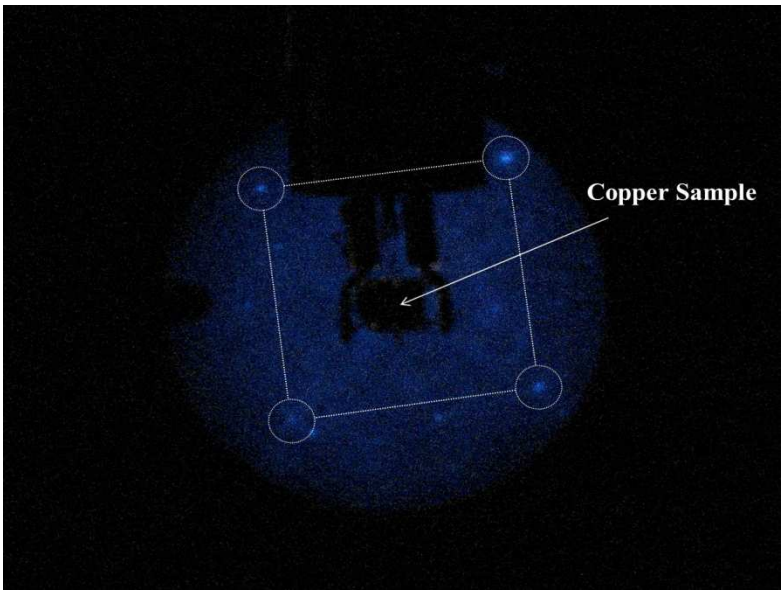

(Figure 5.1) LEED image, taken at ~71 eV electron beam energy, of a copper foil that had been subjected 10 Argon-bombardment and heating cycles.

5.4 *Discussion*

The surface chemistry found on a Cu(111) single crystal surface is identical to that observed on foils that have been cleaned and annealed in UHV. This assertion is supported by the fact that, after ion bombarding and annealing a copper foil several times in UHV, a square (1 x 1) LEED pattern is observed indicating the formation of ordered (100) facets on the surface. This is particularly important for tribological experiments in UHV where it is not feasible to use a single-crystal substrate due to the significant surface damage produced during rubbing.

5.5 *Conclusion*

Both Cu(111) single crystal and vacuum- annealed copper foils can have similar effects on the chemistry of Dimethyl disulfide. LEED experiments show on a polished copper foil after several cycles of argon bombardment and heating, a faint, square (1 x 1) LEED pattern was produced. With further cleaning the square (1 x 1) LEED pattern became significantly sharper. The results suggest that tribological experiments can be conducted on copper foils rather than copper single crystals and produce comparable results.

5.6 *References*

[1] Davey, E.D.; Edwards. E.D. *Wear* **1957**, 1, 291.

[2] Forbes, E.S.; Reid, A. J. D. *ASLE* Trans. **1972**, 16, 50.

[3] Forbes, E.S. *Wear* **1970**, 15, 87.

[4] Allum, K.G.; Forbes, E.S. *J. Inst. Pet*. **1967**, 53, 173

[5] Prutton, C.F.; Turnbull, D.; Dlouhy, G.J. *J. Inst. Pet*. **1946**, 32, 96

[6] Davey, W.J. *J. Inst. Pet*. **1946**, 32, 575.

[7] Spikes, H.A.; Cameron, A. *ASLE Trans*. **1973**, 17, 283.

[8] Bovington, V; Dacre, B ALSE Trans. 1982, 25, 44.

[9] Dacre, B.; Bovington, C.H. *ASLE Trans*. **1982**, 25, 272.

[10] Tomaru, M.; Hironaka, S.; Sakuri, T. *Wear* **1977**, 41, 141.

[11] Murakami, T.; Sakai, T.; Yamamoto, Y.; Hirano, F. *ASLE Trans*. **1985**, 28, 363

[12] Plaza, S.; Mazurkiewiez, B.; Gruzinski, R. *Wear* **1994**, 174, 209.

[13] Plaza, S. *ASLE Trans*. **1987**, 30, 493.

[14] Kajdas, C. *ASLE Trans* **1985**, 28, 21.

Chapter 6: Adsorption of Oxygen and Water and CO Oxidation on Au(111)

6.1 Introduction

Gold, while normally considered to be a noble metal, has been found to have quite remarkable catalytic activity for a number of reactions.[1] In particular, it forms the basis for an active CO oxidation catalyst. While the activity for the direct oxidation of carbon monoxide by adsorbed atomic oxygen can be expected to be high due to the weak bonding of oxygen on gold, it has been found that coadsorbed water on Au(111) facilitates the oxidation of carbon monoxide to carbon dioxide.[2] One of the challenges to studying oxidation chemistry on gold surface in general, and Au(111) in particular, is the low dissociative adsorption probability of molecular oxygen on gold surfaces. One common strategy for studying oxygen adsorption on gold surface in ultrahigh vacuum is to use more reactive ozone rather than O_2. However, exactly because of its reactivity, it is difficult to introduce into ultrahigh vacuum. As described in Chapter 2, an ozone introduction system was built and designed. The following explores the surface reactions of adsorbed oxygen on a Au(111) surface with water and carbon monoxide to further understand the oxidation chemistry and to confirm that the ozone source works properly. This will form the basis for examining model gold-palladium alloy surfaces, which are also active for CO oxidation,[3] but similarly to gold surfaces, dissociative oxygen adsorption on alloys with gold coverages greater than 0.5 ML is very slow.[4]

6.2 Experimental Methods

A Au(111) single crystal (Princeton Scientific) was cleaned with cycles of ion bombardment using 1 keV argon ions for 30 minutes (1 $\mu A/cm^2$), annealing to 900 K for 5 minutes and then to 600 K for 30 minutes. Also the sample was subjected to ozone exposure at a background pressure of 3×10^{-8} Torr for various time periods, then heated to remove carbon and other contaminants from the surface, the ozone configuration is explained more in detail in chapter 2. The sample could be cooled to 80 K by thermal contact to a liquid-nitrogen-filled reservoir and resistively heated to ~1200 K. Ultra-pure H_2O used in these experiments was further purified by several freeze-pump-thaw cycles, the purity was checked with a Dycor Mass spectrometer. The reaction and decomposition products were monitored by TPD.

6.3 Results and Discussion

Oxygen Adsorption from Ozone on Au(111)

The temperature-programmed desorption profiles of an oxygen+ozone mixture is shown in (Figure 6.1). The resulting oxygen desorbs in a sharp peak centered at ~540 K at low coverages and shifts to higher coverages with exposure so that at the highest coverage desorbs at ~560 K. These desorption profiles are in good agreement with previous results on Au(111) [6] where the oxygen was found to desorb at ~520 K at low coverages and ~550 K at saturation. Since the area under the desorption profile is proportional to the oxygen coverage, which has been shown to saturate at 1.2 ML, a plot of oxygen coverage versus exposure can be generated and is shown in (Figure 6.1). This shows an initial, linear uptake of oxygen to a coverage of ~0.9 ML and a slower increase thereafter. This calibration will form the basis for determining coverages in subsequent

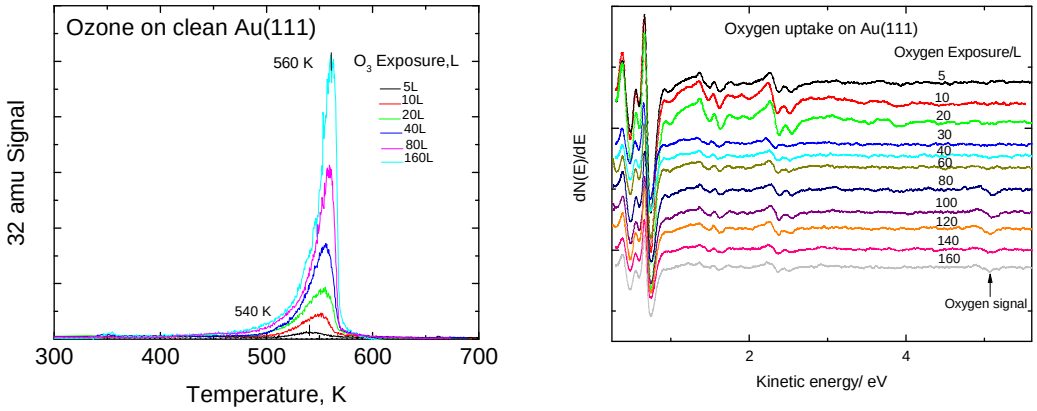

Figure 6.1. (a) TPD profiles collected at 32 amu of a O_2 + O_3 mixture adsorbed on a Au(111) surface at 300 K, collected using a heating rate of 3.4 K/s. The exposures are indicated on the figure. (b) Auger oxygen uptake spectra on Au(111) surface

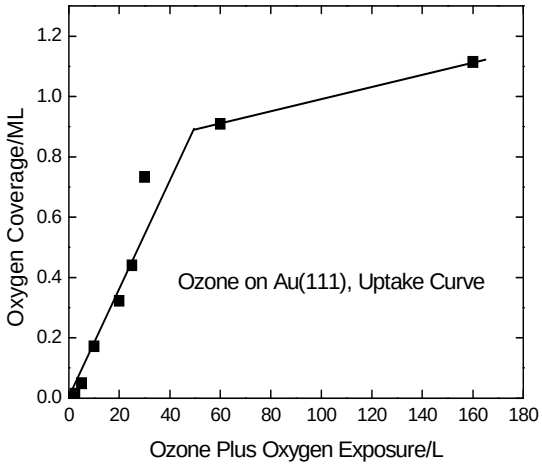

Figure 6.2. Plot of oxygen coverage, measured from the TPD profiles, as a function of exposure to a O_2 + O_3 mixture.

Water Adsorption on Clean and Oxygen-covered Au(111)

The adsorption of water alone on Au(111) is as shown as a function of exposure (in Langmuirs, 1L = 1×10^{-6} Torr s). At the very lowest exposure, the peak temperature is at ~145 K, with a high-temperature tail. As the exposure increases, the peaks temperature increases also so that after an exposure of 1 L has moved to ~153 K. The shift to higher temperatures is ascribed to hydrogen bonding between water molecules and indicates that water adsorbed on the gold surface and the water multilayer desorbs at sufficiently similar temperatures that they cannot be distinguished.

(Figure 6.4) shows the effect of adsorbing water on oxygen-covered Au(111), where the oxygen coverage, formed from ozone, is ~0.5 ML. The desorption profile now differs from that for water alone on Au(111) (Figure 6.3) and initially shows a higher temperature feature centered at ~178 K. This grows with increasing water exposure and saturates after a water exposure of ~2 L, at which point a peak grows at ~158 K due to the desorption of molecular water (Figure 6.3). Experiments using isotopically labeled water and oxygen have shown that the peak at ~178 K is due to the formation of $OH_{(ads)}$ species by reaction of water with adsorbed atomic oxygen, which react by the reverse of the formation reaction to desorb water.[2] The oxygen yield is not affected by this reaction since all of the adsorbed oxygen is recovered as the adsorbed hydroxyl species decompose.

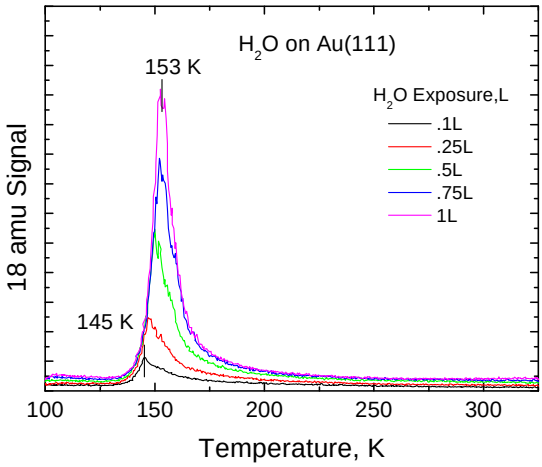

Figure 6.3. TPD profiles collected at 18 amu of water adsorbed on a Au(111) surface at 80 K, collected using a heating rate of 3.4 K/s. The exposures are indicated on the figure.

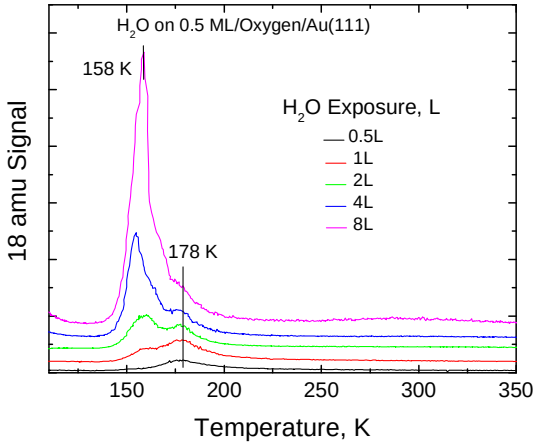

Figure 6.4. TPD profiles collected at 18 amu of water adsorbed on a Au(111) surface covered with 0.5 monolayers of atomic oxygen, at 80 K, collected using a heating rate of 3.4 K/s. The exposures are indicated on the figure.

In order to establish whether all of the oxygen reacts with water to for surface hydroxyl species, experiments were carried out to expose an oxygen-covered surface to water at various sample temperatures (below the desorption temperature of water). The results of this experiment are displayed in (Figure 6.5) and show that the water desorption profile at ~178 K does not vary with the water exposure temperatures suggesting that they have all reacted, or at least have a sufficiently low formation activation barrier that their yield does not change with adsorption temperature.

Carbon Monoxide Oxidation by Oxygen

Some work has been carried out on the oxidation of carbon monoxide on gold surfaces [7,8] but by using molecular beams of carbon monoxide incident on a gold-covered surface. Since carbon monoxide adsorbs very weakly on low-Miller-index gold surfaces, [9-12] although it adsorbed more strongly in step sites, [9] reaction might not be expected to occur in temperature-programmed desorption. Interestingly, therefore, was the observation that adsorbing CO on an oxygen-covered gold surface resulted in the desorption of carbon dioxide at 44 amu (Figure 6.6). This result indicates that carbon monoxide is stabilized by the presence of preadsorbed oxygen on the surface and that it oxidizes to carbon dioxide in two desorption states centered at 120 and 173 K. This indicates that gold is very active for direct oxidation of carbon monoxide through the reaction $CO_{(ads)} + O_{(ads)} \rightarrow CO_{2(g)}$. The strong interaction with the oxygen-covered surface may arise from a direct interaction between adsorbed oxygen and carbon monoxide. Alternatively, oxygen adsorbs by extracting gold atoms from the substrate. [8] Such low-coordination sites can bind oxygen more strongly than the flat surface [13] and may thus provide CO adsorption sites.

Carbon dioxide is formed in two states at 120 and 173 K (Figure 6.5). Their origin is not, at this state clear but it has been shown on copper that oxygen sites on the periphery of oxygen islands are more reactive than isolated sites [14,15] and similar effects may occur on gold.

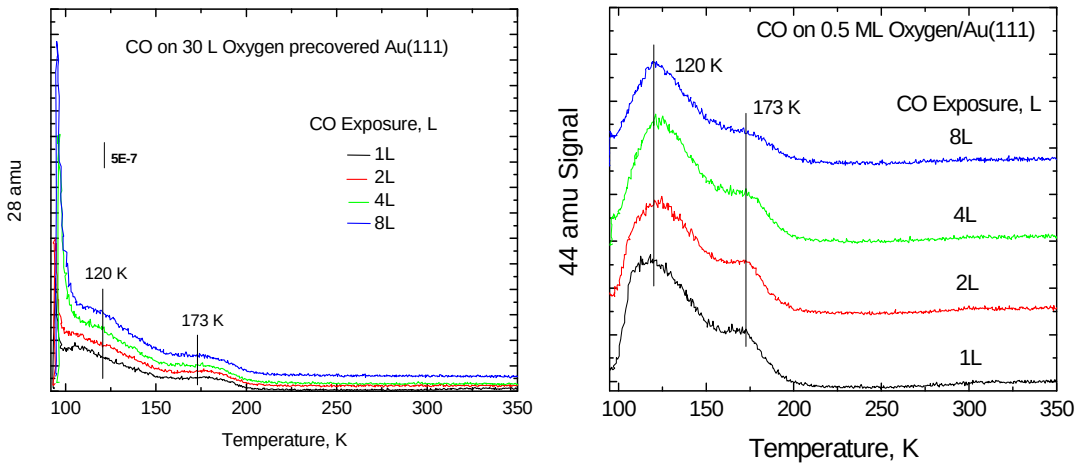

Figure 6.5. TPD profiles collected at 28 and 44 amu of carbon monoxide adsorbed on a Au(111) surface covered with 0.5 monolayers of atomic oxygen, at 80 K, collected using a heating rate of 3.4 K/s. The exposures are indicated on the figure.

Carbon Monoxide Oxidation by Hydroxyl Species

It has been shown that the addition of water to a carbon+oxygen mixture enhances the reaction rate [16,17].The reactivity of surface hydroxyl groups with carbon monoxide has been explored previously [2] where several reaction pathways were identified. The first pathways suggested that CO could react with oxygen that was hydrogen bonded to an adsorbed water molecule, but density functional theory (DFT) calculations indicated that this reaction proceeds with a relatively high activation energy (~32 kJ/mol) and was,

in fact, higher than the reaction with oxygen adsorbed directly to the gold surface because of the additional stabilization energy afforded by the oxygen-water interaction.

This result suggested a direct reaction with surface hydroxyl species. In this case, a spontaneous reaction is found between CO and $OH_{(ads)}$ to form a stable (~177 kJ/mol heat of adsorption) carboxylate (OCOH) species. Several subsequent reactions of this species to form carbon dioxide were explored. Direct hydrogen transfer to the surface is initiated by a *cis-trans* isomerization (with an energy of ~42 kJ/mol) and a subsequent dehydrogenation reaction to yield carbon dioxide and adsorbed hydrogen (with an activation energy of ~89 kJ/mol). A lower activation energy of ~27 kJ/mol is found for hydrogen transfer to an adjacent adsorbed hydroxyl species. The reaction is found to be exothermic by ~205 kJ/mol. Such a low activation barrier would indicate that the reaction will proceed below 80 K (the lowest sample temperature attainable with liquid nitrogen cooling). A lower reaction activation energy (of ~10 kJ/mol) is suggested to occur when the carboxylate species reacts with hydrogen bonded adsorbed hydroxyl species. The low-temperature reaction schemes proposed by Mullins and described above indicate that carbon monoxide should react with surface hydroxyl species to produce molecular water with an activation energy of 10 to 27 kJ/mol depending on the number of adjacent hydroxyl species so that the overall reaction pathway is $CO+2\ OH_{(ads)} \rightarrow CO_2 + H_2O$. Thus, exposure of a hydroxyl-covered surface to carbon monoxide at 80 K should result in the loss of hydroxyl species and the concomitant formation of molecular water. The result of this experiment is shown in (Fig. 6.6), where hydroxyl species are formed by reacting a surface with 0.5 ML of adsorbed atomic oxygen from ozone with water. The initial presence of only hydroxyl species on the surface is indicated by the presence of a single peak at 176 K. As the surface is exposed to more CO, the OH(ads) signal decreases, as expected. A lower-temperature peak, due to molecular water, grows as

expected. However, according the equation given above, the amount of molecular water that is formed is less than the water from hydroxyl species.

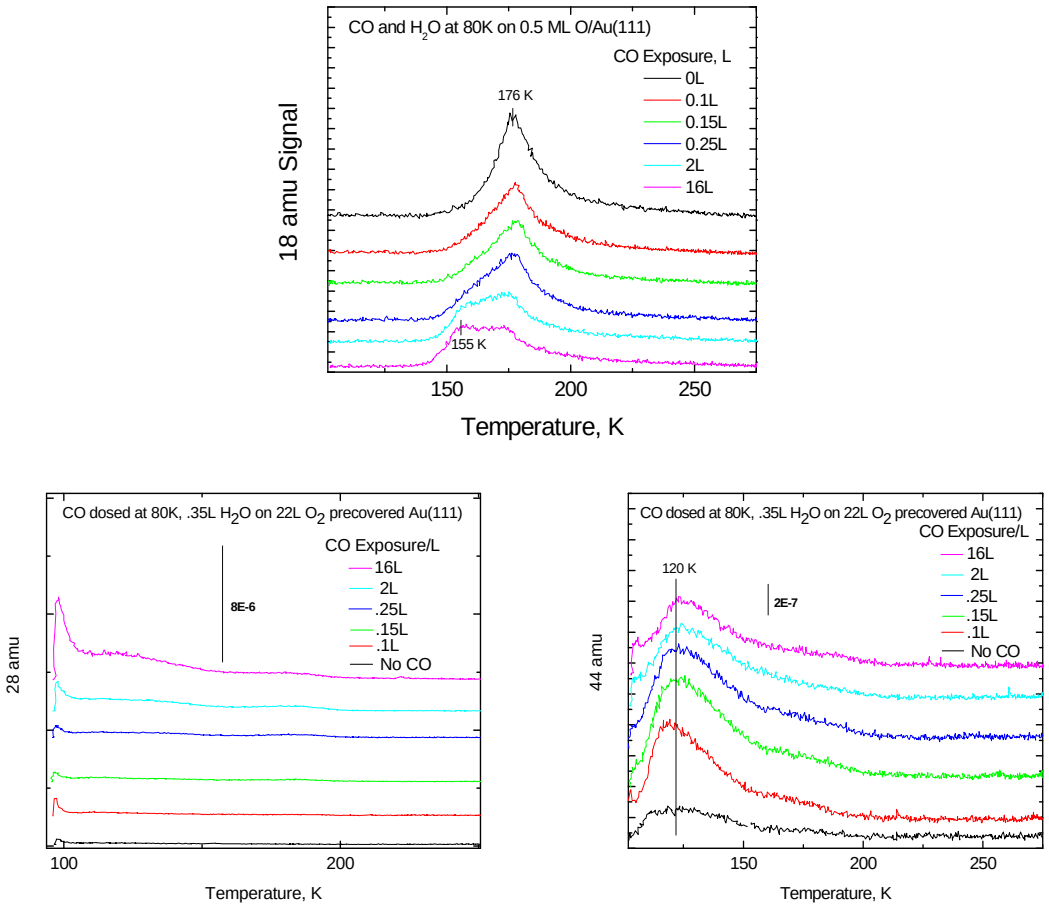

Figure 6.6. TPD profiles collected at 18, 28, and 44 amu following exposure of carbon monoxide to Au(111) surface covered with 0.5 monolayers of atomic oxygen and then exposed to water to form surface hydroxyl groups, at 80 K, collected using a heating rate of 3.4 K/s. The exposures are indicated on the figures.

Since any hydroxyl species present on the surface will decompose to form water and leave atomic oxygen, the atomic oxygen coverage is proportional to the hydroxyl coverage since, as shown above, all surface oxygen species react rapidly with water to form atomic oxygen (which desorbs at ~550 K). The corresponding 32 (O_2) desorption profile is shown in (Figure 6.7), where an inset shows the decrease on oxygen desorption intensity (proportional to the OH(ads) coverage) as a function of CO exposure at 80 K. This indicates that CO does react rapidly with adsorbed hydroxyl species at 80 K as predicted from the DFT calculations. However, the amount of water that is produced by the reaction decreases with CO exposure.

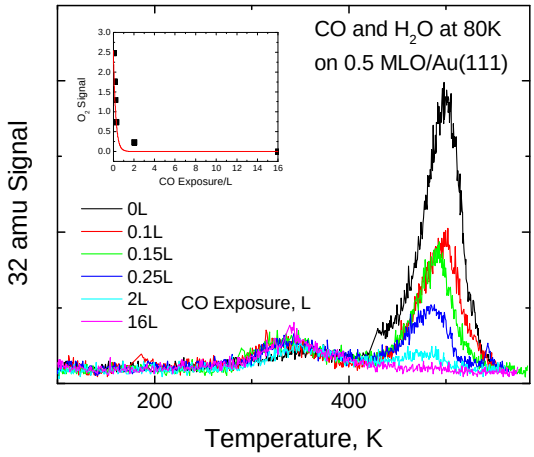

Figure 6.7. TPD profiles collected at 32 amu following exposure of carbon monoxide to Au(111) surface covered with 0.5 monolayers of atomic oxygen and then exposed to water to form surface hydroxyl groups, at 80 K, collected using a heating rate of 5.2 K/s. The exposures are indicated on the figure.

This is emphasized by the plot in (Figure 6.8), which plots the total water yield (both molecular and from surface hydroxyl species) as a function of the coverage of oxygen (from the O_2, 32 amu signal). This shows a linear decrease in the amount of water on the surface with CO exposure, while the total amount of water should remain constant. A possible explanation for this effect is that, although the reaction activation energy is low (~10 to 27 kJ/mol), it is very exothermic (by ~205 kJ/mol). This energy is released at as hydrogen is abstracted from a carboxylate species with surface hydroxyls. Clearly, there is sufficient energy available to cause some of the water that is formed, which, from the TPD data has a heat of adsorption of ~39 kJ/mol, to desorb from the surface. Clearly, not all of the molecular water desorbs and a portion has sufficient time to equilibrate with the cold surface to remain adsorbed until it desorbs at higher temperatures.

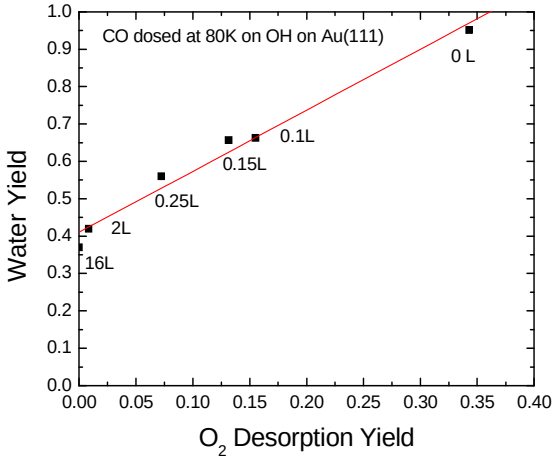

Figure 6.8. Plot of the yield of water against the yield of oxygen following exposure of carbon monoxide to Au(111) surface covered with 0.5 monolayers of atomic oxygen and then exposed to water to form surface hydroxyl groups.

It also appears that the energy released by the reaction of the carboxylate species can cause surface hydroxyl species to desorb water to leave atomic oxygen. This can then react with carbon monoxide to form carbon dioxide at ~120 K (see Figure 6.9). In this experiment, the oxygen coverage was varied and the amount of water was adjusted to just form surface hydroxyl species. Thus the hydroxyl coverage increases in going from spectrum 10A to 10 I. Correspondingly, the coverage of carbon monoxide decreases due to site blocking. This indicates that atomic oxygen is formed on the surface by reaction with CO since the carbon dioxide desorption temperature (~120 K) is identical to that found when the surface is dosed onto with oxygen (Figure 6.6). However, in this case, the 173 K feature seen in (Figure 6.6) is much weaker. This CO_2 is clearly the result of oxygen formed from surface hydroxyl species since the trend with hydroxyl coverage is what would be expected for a reaction wit surface CO. At the highest coverage (Figure 6.9 I), no CO_2 is formed since CO adsorption is completely blocked. As the hydroxyl coverage decreases slightly (Figure 6.9 H), carbon dioxide is detected. An additional state appears at ~109 K and a simple Redhead analysis [18] suggests that this would correspond to a desorption activation energy of ~27 kJ/mol, close to the value for reaction of the carboxylate with isolated surface hydroxyl species. The intensity of the CO_2 desorption state reaches a maximum at a hydroxyl coverage of ~1 ML and decreases at lower coverage. These results provide convincing evidence that the surface oxygen derives from the $OH_{(ads)}$ species originally on the surface, but that they for adsorbed oxygen species that then react with CO to form CO_2 at ~120 K. Adsorbed atomic oxygen is clearly formed at some stage of the reaction with CO, although this is not a product in the stoichiometric reaction. The most plausible explanation is that the larger exothermicity of the reaction between surface hydroxyl groups and a carboxylate species dissipates sufficient energy to cause molecular water to desorb (Figure 6.9) and the decomposition of some surface hydroxyl groups.

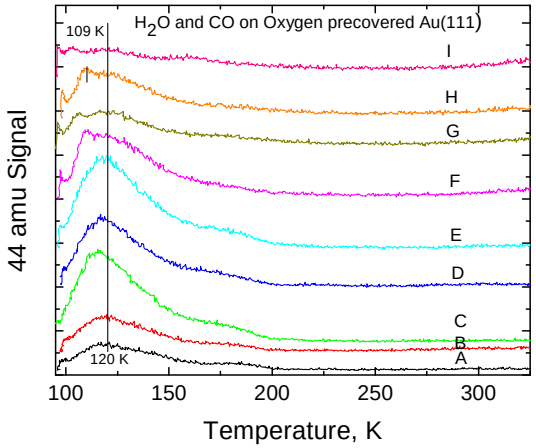

Figure 6.9 TPD profiles collected at 44 amu following exposure of carbon monoxide to Au(111) surface covered with atomic oxygen and then exposed to water to form surface hydroxyl groups, collected using a heating rate of 3.4 K/s. A. 4L O_2, 0.05L H_2O, .25L CO (θ(OH)= 0.12 ML), B. 8L O_2, 0.1L H_2O, 0.5L CO (θ(OH)= 0.29 ML), C. 11L O_2, 0.2L H_2O, 0.6L CO (θ(OH)= 0.41 ML), D. 15L O_2, 0.25L H_2O, 0.75L CO (θ(OH)= 0.56 ML), E. 22L O_2, 0.35L H_2O, 0.85L CO (θ(OH)= 0.82 ML), F. 30L O_2, 0.5L H_2O, 1L CO (θ(OH)= 1.11 ML), G. 45L O_2, 0.65L H_2O, 1.25L CO (θ(OH)= 1.67 ML), H. 60L O_2, 0.75L H_2O, 1.5 L CO (θ(OH)= 1.8 ML), I. 100L O_2, 1L H_2O, 1.75L CO (θ(OH)= 2.0 ML).

7.4 *Conclusions*

Reactive ozone is used to deposit oxygen onto an Au(111) single crystal surface, which it was found that this O_2 species desorbs at ~ 560K under UHV conditions using Temperature programmed desorption. It was also found that CO and O_2 coadsorbed on the Au(111) surface forms two CO_2 desorption states, the first low temperature state at 120K and a higher temperature state at 173K. H_2O is added to the oxygen precovered

Au(111) surface to form OH hydroxyl groups on the surface which desorb at 178K, and a lower temperature peak at 158K corresponds to molecular water desorbing from the surface. H_2O species added with carbon monoxide on oxygen precovered Au(111) showed to have an effect on peak temperature in carbon dioxide desorption in TPD. There was one initial low temperature desorption peak at 120K without the addition of H_2O. As H_2O was introduced at a coverage of 0.5L on 30L of oxygen and 1L of carbon monoxide coadsorbed a second low temperature desorption peak began to form at 109K , which indicates a more reactive site. This proves that H_2O has an effect on carbon monoxide oxidation on Au(111) single crystal surface. As the surface is exposed to more CO, the OH(ads) signal decreases, as expected. A lower-temperature peak, due to molecular water, grows as expected. However, according the equation given above, the amount of molecular water that is formed is less than the water from hydroxyl species. As the amount of CO desorbed on the surface decreases the amount of CO_2 produced also decreases. The amount of oxygen decreases rapidly and is completely depleted as the exposure of CO is increased. The amount of water is also decreased although a small amount of molecular water remains on the surface after the reaction occurs. Further investigation is needed to hone in on other possible reaction mechanisms.

7.5 References

[1] Haruta, M.; Yamada, N.; Kobayashi, T.; Iijima, S. *Journal of Catalysis* **1989**, *115*, 301.

[2] Ojifinni, R. A.; Froemming, N. S.; Gong, J.; Pan, M.; Kim, T. S.; White, J. M.; Henkelman, G.; Mullins, C. B. *Journal of the American Chemical Society* **2008**, *130*, 6801.

[3] Li, Z.; Gao, F.; Tysoe, W. T. *The Journal of Physical Chemistry C* **2010**, *114*, 16909.

[4] Boscoboinik, J. A.; Calaza, F. C.; Garvey, M. T.; Tysoe, W. T. *The Journal of Physical Chemistry C* **2010**, *114*, 1875.

[5] Boscoboinik, J. A.; Calaza, F. C.; Habeeb, Z.; Bennett, D. W.; Stacchiola, D. J.; Purino, M. A.; Tysoe, W. T. *Physical Chemistry Chemical Physics* **2010**, *12*, 11624.

[6] Saliba, N.; Parker, D. H.; Koel, B. E. *Surf. Sci.* **1998**, *410*, 270.

[7] Michael Gottfried, J.; Christmann, K. *Surf. Sci.* **2004**, *566–568, Part 2*, 1112.

[8] Min, B. K.; Alemozafar, A. R.; Pinnaduwage, D.; Deng, X.; Friend, C. M. *The Journal of Physical Chemistry B* **2006**, *110*, 19833.

[9] Kim, J.; Samano, E.; Koel, B. E. *J. Phys. Chem. B* **2006**, *110*, 17512.

[10] Kottke, M. L.; Greenler, R. G.; Tompkins, H. G. *Surf. Sci.* **1972**, *32*, 231.

[11] Piccolo, L.; Loffreda, D.; Aires, F.; Deranlot, C.; Jugnet, Y.; Sautet, P.; Bertolini, J. C. *Surf. Sci.* **2004**, *566*, 995.

[12] Ruggiero, C.; Hollins, P. *Journal of the Chemical Society, Faraday Transactions* **1996**, *92*, 4829.

[13] Janssens, T. V. W.; Clausen, B. S.; Hvolbaek, B.; Falsig, H.; Christensen, C. H.; Bligaard, T.; Norskov, J. K. *Top. Catal.* **2007**, *44*, 15.

[14] Crew, W. W.; Madix, R. J. *Surf. Sci.* **1996**, *356*, 1.

[15] Crew, W. W.; Madix, R. J. *Surf. Sci.* **1996**, *349*, 275.

[16] Daté, M.; Haruta, M. *Journal of Catalysis* **2001**, *201*, 221.

[17] Daté, M.; Okumura, M.; Tsubota, S.; Haruta, M. *Angewandte Chemie International Edition* **2004**, *43*, 2129.

[18] Redhead, P. A. *Vacuum* **1962**, *12*, 203.